The SEGUE Stellar Parameter Pipeline. I. Description and Initial Validation Tests

Young Sun Lee, Timothy C. Beers, Thirupathi Sivarani

Department of Physics & Astronomy,
CSCE: Center for the Study of Cosmic Evolution,
and JINA: Joint Institute for Nuclear Astrophysics,
Michigan State University, East Lansing, MI 48824, USA

lee@pa.msu.edu, beers@pa.msu.edu, thirupathi@pa.msu.edu

Carlos Allende Prieto, Lars Koesterke

Department of Astronomy,
University of Texas, Austin, TX 78712

callende@astro.as.utexas.edu

Ronald Wilhelm

Department of Physics,
Texas Tech University, Lubbock, TX 79409

ron.wilhelm@ttu.edu

John E. Norris

Research School of Astronomy and Astrophysics,
The Australian National University, Weston, ACT 2611, Australia

jen@mso.anu.edu.au

Coryn A. L. Bailer-Jones, Paola Re Fiorentin

Max-Planck-Institute für Astronomy, Königstuhl 17, D-69117, Heidelberg, Germany

calj@mpia-hd.mpg.de, fiorent@mpia-hd.mpg.de

Constance M. Rockosi

Department of Astronomy,
University of California, Santa Cluz, CA 95064

crockosi@ucolick.org

Brian Yanny

Fermi National Accelerator Laboratory,
Batavia, IL 60510

yanny@fnal.gov

Heidi J. Newberg

Department of Physics & Astronomy,
Rensselaer Polytechnical Institute, Troy, NY 12180

newbeh@rpi.edu

Kevin R. Covey

Harvard-Smithsonian Center for Astrophysics,
60 Garden Street, Cambridge, MA 02138

kcovey@cfa.harvard.edu

ABSTRACT

We describe the development and execution of the SEGUE Stellar Parameter Pipeline (SSPP), which makes use of multiple techniques in order to estimate the fundamental stellar atmospheric parameters (effective temperature, $T_{\rm eff}$, surface gravity, $\log g$, and metallicity, parameterized by [Fe/H]) for stars with spectra and *ugriz* photometry obtained during the course of the original Sloan Digital Sky Survey (SDSS-I) and its first extension (SDSS-II/SEGUE). The use of multiple approaches allows for an empirical determination of the internal errors for each derived parameter, based on the range of the reported values from each method. Based on about 120,000 spectra for stars obtained during SDSS-I and SEGUE that satisfy $S/N \geq 10/1$ (average value over the spectra range 3,850-6,000 Å, and have derived temperatures in the range 4500 K $\leq T_{\rm eff} \leq$ 7,500 K, typical internal errors obtained by the SSPP are $\sigma(T_{\rm eff}) \leq 75$ K, $\sigma(\log\ {\rm g}) \leq 0.20$ dex, and $\sigma([{\rm Fe/H}]) \leq 0.10$ dex.

A comparison with an analysis of high-resolution spectra for over 150 SDSS-I/SEGUE stars suggests that the SSPP is able to estimate $T_{\rm eff}$, $\log g$, and [Fe/H] to an external uncertainty (random plus systematic errors) of 117 K, 0.26 dex, and 0.22 dex, respectively, in the temperature range 4500 K $\leq T_{\rm eff} \leq$ 7,500 K. These errors apply for the very highest S/N spectra obtained from SDSS ($S/N >$

50/1), as only quite bright stars were targeted for high-resolution observations. Outside of the quoted temperature range, we presently to do not have sufficient high-resolution spectra to fully test the parameters obtained by the SSPP.

An analysis of likely member stars in a handful of Galactic open and globular clusters indicates that the SSPP slightly over-estimates [Fe/H] (by on the order of 0.15 dex) for stars with [Fe/H] < -2.0, and under-estimates [Fe/H] for stars with near solar metallicities by ~ 0.3 dex. Determinations of $T_{\rm eff}$ and log g exhibit no obvious offsets relative to expectations. Despite these small remaining uncertainties, the SSPP determines stellar atmospheric parameters with sufficient accuracy and precision, in the temperature range 4500 K $\leq T_{\rm eff} \leq$ 7,500 K, to carry out detailed explorations of the chemical compositions and kinematics of the thick-disk and halo populations of the Milky Way.

Subject headings: methods: data analysis — stars: abundances, fundamental parameters — surveys — techniques: spectroscopic

1. Introduction

The Sloan Extension for Galactic Understanding and Exploration (SEGUE) is one of three surveys that are being executed as part of the current extension of the Sloan Digital Sky Survey (SDSS-II), which consists of LEGACY, SUPERNOVA SURVEY, and SEGUE. The SEGUE program is designed to obtain *ugriz* imaging of some 3,500 square degrees of sky outside of the original SDSS-I footprint (Fukugita et al. 1996; Gunn et al. 1998, 2006; York et al. 2000; Stoughton et al. 2002; Abazajian et al. 2003, 2004, 2005; Pier et al. 2003; Adelman-McCarthy et al. 2007a). The regions of sky targeted are primarily at lower Galactic latitudes ($|b| < 35^{\circ}$) in order to obtain the data required to better understand the disk/halo interface of the Milky Way. At the time of this writing, about 85% of the planned additional imaging has already been completed. SEGUE is also obtaining $R \simeq$ 2,000 spectroscopy over the wavelength range 3,800-9,200 Å for some 250,000 stars in 200 selected areas over the sky available from Apache Point, New Mexico. The spectroscopic candidates are selected on the basis of *ugriz* photometry to populate roughly 16 target categories, chosen to explore the nature of the Galactic stellar populations over distances from 0.5 kpc to over 100 kpc from the Sun. Spectroscopic observations have been obtained for roughly half of the planned targets thus far, for a total of about 120,000 spectra. The SEGUE data clearly require automated analysis tools in order to efficiently extract the maximum amount of useful astrophysical information for the targeted stars, in particular their stellar atmospheric parameters, over wide ranges of the effective temperature ($T_{\rm eff}$), surface gravity (log g), and metallicity, [Fe/H].

Numerous methods have been developed in the past in order to extract atmospheric parameter estimates from medium-resolution stellar spectra in a fast, efficient, and automated fashion. These approaches include techniques for finding the minimum distance (parameterized in various ways) between observed spectra and grids of synthetic spectra (see, e.g., Allende Prieto et al. 2006), non-linear regression models (e.g., Re Fiorentin et al. 2007 and references therein), correlations between broadband colors and the strength of prominent metallic lines, such as the Ca II K line (Beers et al. 1999), auto-correlation analysis of a stellar spectrum (Beers et al. 1999, and references therein), obtaining fits of spectral lines (or summed line indices) as a function of broadband colors (Wilhelm et al. 1999), or the behavior of the Ca II triplet lines as a function of broadband color (Cenarro et al. 2001a,b). However, each of these approaches exhibits optimal behavior only over restricted temperature and metallicity ranges; outside of these regions they are often un-calibrated, suffer from saturation of the metallic lines used in their estimates at high metallicity or low temperatures, or lose efficacy due to the weakening of metallic species at low metallicity or high temperatures. The methods that make use of specific spectral features are susceptible to other problems, e.g., the presence of emission in the core of the Ca II K line for chromospherically active stars, or poor telluric line subtraction in the region of the Ca II triplet. Because SDSS stellar spectra cover most of the the entire optical wavelength range, one can apply several approaches, using different wavelength regions, in order to derive estimates of stellar parameters. The combination of techniques results in estimates of stellar parameters that are more robust over a much wider range of $T_{\rm eff}$, log g, and [Fe/H] than those that might be derived by individual methods. The SEGUE Stellar Parameter Pipeline (hereafter, SSPP) described herein implements this "multi-method" philosophy. We also carry out a number of tests in order to assess the range of stellar atmospheric parameter space over which the estimates obtained by the SSPP remain valid.

Section 2 describes determinations of radial velocity used by the SSPP. The procedures used to obtain an estimate of the appropriate continuum, and the determination of line indices is explained in §3. The methods that the SSPP employs for determining stellar parameters are described in §4. Section 5 addresses the determinations of auxiliary estimates of effective temperature, based on both theoretical and empirical approaches; these methods are used for stars where adequate estimates of $T_{\rm eff}$ are not obtained by our primary techniques. A decision tree that obtains the optimal set of parameter estimates based on the multiple methods is described in §6. Section 7 summarizes the conditions for raising various flags to warn potential users where uncertainties in parameter determinations remain. In §8, we discuss validation of the parameters determined by the SSPP based on SDSS-I/SEGUE stars for which we have obtained higher dispersion spectroscopy on various large telescopes, and also compare the parameters with those of likely member stars of Galactic open and

globular clusters. Assignments of approximate MK spectral classifications are described in §9. In §10 we describe several methods for the determination of distances used by the SSPP. Section 11 presents a summary and conclusions. Note that the colors ($u-g$, $g-r$, $r-i$, $i-z$, and $B-V$) and magnitudes ($u,\ g,\ r,\ i,\ z,\ B,$ and V) are understood to be de-reddened and corrected for absorption (using the dust maps of Schlegel et al. 1998), unless stated specifically otherwise.

2. Determinations of Radial Velocities

2.1. The Adopted Radial Velocities Used by the SSPP

The *spZbest* fits file, which is generated from the SDSS spectroscopic reduction pipeline, provides two estimated radial velocities. One is an absorption-line redshift derived from a cross-correlation procedure using templates that were obtained from SDSS commissioning spectra (Stoughton et al. 2002). Another estimate comes from performing a "best-match" procedure that compares the observed spectra with externally measured templates (in this case, the ELODIE library high-resolution spectra, as described by Prugniel & Soubiran 2001 and Moultaka et al. 2004), degraded to the resolving power of SDSS spectra.

Previous experience with the analysis of SDSS stellar spectra suggested that the radial velocity estimated from the ELODIE template matches is often the best available estimate, in the sense that it is the most repeatable based on spectra of "quality assurance" stars with multiple determinations. However, these are some cases where the quoted error of an ELODIE spectral match velocity is larger than expected, so we also make use of the cross-correlation radial velocity, in the following manner. If the velocity determined by comparison with the ELODIE templates has a reported error of 20 km s^{-1} or less, then this velocity is adopted and the radial velocity flag is set to 'RVOK(20)'. If the error from the ELODIE template comparison is larger than 20 km s^{-1} and the relative difference between the two reported radial velocities is less than 40 km s^{-1}, then we take an average of the two techniques, and the radial velocity flag is set to 'RVOK(40) '. If the error in the reported ELODIE velocity is larger than 20 km s^{-1}, and the difference of between the two estimates is between 40 and 100 km s^{-1}, we take an average of the two and the radial velocity flag is set to 'RVOK(100)'.

If none of the above conditions are satisfied (which happens only rarely, and mainly for quite low S/N spectra, or for hot/cool stars without adequate templates), then we obtain an independent estimate of the radial velocity based on our own IDL routines. The calculation of the radial velocity is carried out by determining wavelength shifts for several

strong absorption line features (Ca II K, Ca II H, Hδ, Ca I, Hγ, Hβ, Na I, Hα, the Ca II triplet). After ignoring the calculated velocity above +500 km s^{-1} or below -500 km s^{-1} from the individual lines (which are very often spurious), we obtain a 3σ clipped average of the remaining radial velocities. If this computed average falls between -500 km s^{-1} and +500 km s^{-1}, we take the calculated radial velocity as the adopted radial velocity and set the radial velocity flag to 'RVCALOK'.

It should be noted that many of the techniques used for atmospheric parameter estimation in the SSPP work well even when the velocity determination for a given star has errors of up to 100 s^{-1} or more. Hence, we choose not to ignore spectra with high velocity errors, but rather simply indicate caution with the appropriate radial velocity flag.

If none of the above methods yield an acceptable estimate of radial velocity, or if the reported velocity is apparently spurious (greater than 1000 km s^{-1} or less than $-1,000$ km s^{-1}), we simply ignore the spectrum of the star in our subsequent analysis, and set the radial velocity flag to 'RVNOTOK'.

2.2. Checks on Radial Velocities – Zero Points and Scatter

To check on the accuracy of the SSPP radial velocities, we compare with the sample of over 150 high-resolution spectra of SDSS-I/SEGUE stars that have been obtained in order to calibrate and validate the stellar atmospheric parameters obtained by the SSPP. Table 1 summarizes the high-resolution data available to date. We plan to continue enlarging this sample of validation stars in the near future.

The high-resolution spectra have been reduced and analyzed independently by two of the present authors (T.S. and C.A.). A detailed discussion is presented by Allende Prieto et al. (2007). During the course of deriving the stellar parameter estimates from the high-resolution spectra, the radial velocities of stars are first measured. Note that C.A. only considered the HET spectra, while S.T. considered all available spectra. So, only the HET stars have radial velocities obtained by both analysts; for these stars we take an average of their independent determinations, which typically differ by no more than 1-2 km s^{-1}.

After rejecting problematic spectra (e.g., low S/N high-resolution spectra, or stars that appear to be spectroscopic binaries at high spectral resolution), 137 stars remain to compare with the radial velocity results obtained for the medium-resolution SDSS spectra with the SSPP. Figure 1 shows the the results of these comparisons. A consistent offset of about -6.6 km s^{-1} (with a standard deviation of 5.2 km s^{-1}) is obtained from a Gaussian fit to the residuals; this offset appears constant over the color range $0.1 \leq g - r \leq 0.9$. An

additional comparison with the radial velocity distribution of likely member stars in the Galactic globular clusters M 15 and M 13 reveals similar offsets (-6.8 km s^{-1} and -8.6 km s^{-1}, respectively; see Lee et al. 2007b for a more detailed analysis). The origin of this velocity offset has not yet been identified, but we expect that it may be tied to the wavelength solutions obtained for the individual fibers. However, in order to account for its presence, we apply an empirical $+7.3$ km s^{-1} shift (the mean of the offsets from analysis of the high-resolution and the globular-cluster data), to each radial velocity obtained by the SSPP. For the time being, we conclude that the zero-point uncertainties in the corrected radial velocities determined by the SSPP (and the SDSS spectroscopic reduction pipeline it depends on) should be close to zero, with scatter on the order of 5 km s^{-1}. Note that the scatter in the determination of radial velocities, based on the average displacements of the 'quality assurance' stars with multiple measurements, varies from 3.5 km s^{-1} (for brighter stars) to 20 km s^{-1} (for fainter stars).

3. Calculations of Line Indices

The initial step in calculation of line indices for SDSS spectra is to transform the wavelength scale of the original SDSS spectrum over to an air-based (rather than vacuum-based) wavelength scale, and to linearly rebin the spectrum to 1 Å bins in the blue (3,800-6,000 Å), and 1.5 Å bins in the red (6,000-9,000 Å). Then, based on the adopted radial velocity described above, the wavelength scale is shifted to zero rest wavelength.

The SSPP measures 77 atomic and molecular lines. Line index calculations are performed in two modes; one is to use a global continuum fit over the entire wavelength range (3,850-9,000 Å), the other is to obtain a local continuum around the line bands of interest. The choice between which mode is used depends on the line depth and width of the feature under consideration. Local continua are employed for the determinations of stellar atmospheric parameters based on techniques that depend on individual line indices. Other techniques, such as the neural network, spectral matching, and autocorrelation methods, require wider ranges to be considered; for these the global continuum is used. We make use of the errors in the fluxes reported by the SDSS spectroscopic reduction pipeline in order to obtain estimates in the uncertainties in the line indices. Details of the procedures used to obtain the continuum fits and line index measures (and their errors) are discussed in this section.

3.1. Continuum Fit Techniques

3.1.1. Global Continuum Fit

Determination of the appropriate continuum for a given spectrum is a delicate task, even more so when it must be automated, and obtained for stars having wide ranges of effective temperatures, as is the case for the present application.

In order to obtain a global continuum fit, the SSPP first proceeds by fitting the stellar spectrum to a seventh order polynomial. For wavelengths less than 6,500 Å, if the observed flux is below that of the initial continuum fit in each pixel, we add the difference between the observed flux and initial continuum fit to the value of the continuum fit at each pixel. For wavelengths larger than 6,500 Å, we overwrite the observed flux with the fitted continuum function (plus errors). This modified flux vector becomes the input for the next continuum estimate, again obtained by fitting a seventh order polynomial. This loop is iterated twice. The resultant continuum is considered the first pass estimate of the global continuum level.

The reason for setting the wavelength cut to 6,500 Å in the above algorithm is to guard against the effects of, e.g., low signal-to-noise data in the red for warmer stars, the peculiar flux distribution of extremely cool stars, or poor sky line subtraction around the Ca II triplet in the SDSS pipeline (in some cases). We find that if we use the filtered flux for the first-pass continuum estimate, as above, we are better able to obtain reasonable results in the red portion of the spectrum.

After obtaining the first-pass estimated continuum, we reject points in the modified flux vector that are more than 3σ above the fitted continuum, where σ is the estimated error in the fitting function. Then, a sixth order polynomial fit to the 3σ-clipped flux is carried out in order to obtain a second-pass continuum estimate. The final global continuum level is determined from a weighted sum of the two estimated continua (40% of the first-pass continuum level estimate is added to 60% of the second-pass continuum level estimate). The upper panel of Figure 2 shows an example of a fitted global continuum obtained in this manner. The bottom panel is the normalized spectrum, obtained by division of the spectrum by the global continuum fit. It can be seen that a reasonable continuum estimate is obtained even in the region of the Ca II triplet, where residuals from poor sky subtraction can sometimes be problematic.

3.1.2. Local Continuum Fit

To obtain a local continuum over the line band of interest, we first calculate a 5σ-clipped average of the fluxes over the (blue and red) sidebands corresponding to each feature, as listed in Table 2. From an average of these values a linear interpolation procedure is carried out over the central line band. This linearly interpolated flux is then connected piecewise with the average fluxes of the red and blue sidebands, and a robust fit is performed over the entire region of the blue sideband + line band + red sideband to derive the final local continuum estimate.

3.2. Computation of Line Indices

Line indices (or equivalent widths) are calculated by integrating a continuum normalized flux over the specified wavelength regions of each line band. Two different measurements of line indices, obtained from the from two different continuum methods described above, are reported, even though the line-index based methods for stellar parameter estimates only make use of the local continuum-based indices. In order to avoid spurious values for the derived indices, if a given index measurement is greater than 100 Å, or is negative, we set the reported value to −9.999. No parameter estimates based on that particular line index are estimated.

Table 2 lists the complete sets of line indices made use of in the SSPP. However, it should be noted that, unlike the case for most of the features in this Table, the line indices listed in rows 74 (TiO1), 75 (TiO2), 76 (TiO3), 77 (TiO4), 78 (TiO5), 79 (CaH1), 80 (CaH2), 81 (CaH3), 82 (CaOH), and 83 (Hα) are calculated following the prescription given by the HAMMER program (Covey et al. 2007). The line index for Ca I at 4,227 Å and the Mg Ib/H features around 5,170 Å are computed following Morrison et al. (2003), in order for them to be used to estimate log g as described in Section 4.4.

We follow the Cayrel (1988) procedure to compute an error for each line index measurement. The uncertainty (W_{error}) in the index or measured equivalent width is:

$$W_{error} = \frac{1.6 \times (resolution \times pixel\ size)^{1/2}}{SNR} \quad (1)$$

where SNR is signal-to-noise ratio in the local region of the spectrum, the *resolution* is taken to be ~ 2.5 Å, and the *pixel size* is set to 1 Å. The noise spectrum provided by the SDSS spectroscopic reduction procedure is used to compute the local SNR.

4. Methodology

The SSPP employs a number of methods in order to estimate effective temperature, surface gravity, and metallicity from SDSS spectroscopy and photometry. In this section, each method used in the SSPP is summarized. Since many of the methods implemented in the SSPP are already described by previously published papers, we will address those techniques briefly, and refer the reader to individual papers for detailed descriptions. Those methods that are introduced here for the first time are explained in more detail. Note that some approaches estimate all three atmospheric parameters simultaneously, while others are specific to an individual parameter.

4.1. Spectral Fitting With the `k24` and `ki13` Grids

These two methods are based on identification of the parameters for a model atmosphere that best matches the observed fluxes in a selected wavelength interval. This method is described in detail by Allende Prieto et al. (2006). Classical LTE line-blanketed model atmospheres are used to compute a discrete grid of fluxes, and interpolation allows subgrid resolution. The search is performed using the Nelder-Mead algorithm (Nelder & Mead 1965).

The same grid described by Allende Prieto et al. (2006) is used in the SSPP. We refer to this set of model fluxes as the `k24` grid. It includes a predicted broadband color index $(g-r)$, as well as normalized spectral fluxes in the region 4,400-5,500 Å at a resolving power of $R = 1000$. Kurucz (1993) model atmospheres and very simple continuum opacities are used to calculate synthetic spectra. The broadband photometry was derived from the spectral energy distributions provided by Kurucz (1993) and the passbands determined by Strauss & Gunn (2001) for point sources and an airmass of 1.3.

In addition to the `k24` grid, a second grid, referred to as `ki13`, is now implemented in the SSPP. This second grid covers the same spectral window as `k24`, but *no photometry* is considered. The use of only the derived normalized spectra de-couples the results based on this grid from reddening and photometric errors, although valuable information, mainly on surface temperature, is somewhat sacrificed.

There are several other differences between the `k24` and `ki13` grids. The new grid includes molecular line opacities, with the most relevant molecules in the range of interest being the CH G band near 4,300 Å) as well as the MgH band. In addition, the `ki13` grid takes advantage of a novel concept that allows for a significant increase in the speed of these calculations. The relevant opacities are not calculated for all depths in all models, but instead are obtained on a temperature and density grid, and later interpolated to the exact

points in any given model atmosphere. The opacity grid includes 4 points per decade in density and steps of 125 K in temperature. With these choices, linear interpolation leads to errors in the derived normalized fluxes < 1 %.

Allende Prieto et al. (2006) made use of several libraries of observed spectra and atmospheric parameters to study systematic and random errors obtained from the `k24` analysis. Even at infinite signal-to-noise ratios, random errors appear significantly larger than systematic errors, and amount to 3% in $T_{\rm eff}$, 0.3 dex in $\log g$, and 0.2 dex in [Fe/H]. This is most likely the result of over-simplified model fluxes with a solar-scaled abundance pattern (including an enhancement of the α elements at low iron abundance), which is too limited to account for the chemical spread in real stars. The new `ki13` grid offers a significant improvement in random errors, which at high signal-to-noise amount to 2 % in $T_{\rm eff}$, 0.2 dex in $\log g$, and 0.1 dex in [Fe/H], but a less robust behavior, due to the lack of color information, at low signal-to-noise ratios.

As discussed in Allende Prieto et al. (2006), the `k24` and `ki13` approaches perform best in the range 5,000 K $\leq T_{\rm eff} \leq$ 7,000 K, which corresponds to $0.1 \leq g - r \leq 0.7$; the SSPP restricts the adopted parameters from these methods to this color range. These methods are designated in the SSPP according to the following: the $T_{\rm eff}$, $\log g$, and [Fe/H] estimated with the `k24` are referred to as T9, G7, and M8, respectively, while these parameters estimated from the `ki13` grid are referred to as T10, G8, and M9, respectively.

4.2. The Ca II K method, and the Auto-Correlation Function Method

These methods are based on the procedures outlined by Beers et al. (1999), where the interested reader should look for more details. A brief summary follows.

The Ca II K method makes use of a "band-switched" estimate of the pseudo-equivalent of the Ca II K line at 3,933 Å, in combination with an estimate of a broadband color, to obtain a prediction of the [Fe/H] for a given star. The approach has been used for two decades during the course of the HK (Beers, Preston, & Shectman 1985, 1992) and the Hamburg/ESO objective prism surveys (Reimers & Wisotzki 1997; Christlieb 2003) for the determination of metallicities of stars with available medium-resolution (2–3 Å resolution, similar to the resolution of the SDSS spectra) follow-up spectroscopy. The original calibration is based on high-resolution abundance determinations (and $B - V$ colors) for a sample of $\sim$ 500 stars. It is clear that one adopts the assumption that the calcium abundance tracks the iron abundance in a monotonic fashion, which is almost always valid. In the process of deriving the estimate of [Fe/H], the relationship between [Fe/H] and [Ca/Fe] used is as

follows:

$$[\mathrm{Ca/Fe}] = \begin{cases} 0 & \text{if } [\mathrm{Fe/H}] \geq 0 \\ -0.267\times\ [\mathrm{Fe/H}] & \text{if } -1.5 \leq [\mathrm{Fe/H}] < 0 \\ +0.4 & \text{if } [\mathrm{Fe/H}] < -1.5 \end{cases} \quad (2)$$

This method has been shown to perform well over a wide range of metallicities, in particular for stars with [Fe/H] < -1.0; external errors from the calibration indicate that it has an intrinsic error no greater than 0.15–0.20 dex in the color range $0.3 \leq B - V \leq 1.2$. Above [Fe/H] $= -1.0$, and in particular for cooler stars (below $T_{\rm eff} = 5{,}000$ K), the Ca II K line gradually begins to saturate. As a result, for cool, metal-rich stars, the method will generally return an estimate of [Fe/H] that is on the order of 0.5 dex too low. This is ameliorated somewhat by empirical corrections that are built in to the program used to calculated this estimate, but it remains a source of concern. It is important to recognize that for stars with very low metallicities, and for warmer stars in particular, the Ca II K line is one of the few (in some cases only) metallic lines available in medium-resolution spectra of the sort we are working with. Hence, this estimator plays an especially important role in such situations.

Clearly, in the present application, a measurement of $B - V$ is not available. Hence, we used the observed (or predicted, when necessary) $g - r$ color to estimate the $B - V$ color. In order to accomplish this task, we made use of several hundred stars with existing $B - V$ colors obtained during the course of the HK and Hamburg/ESO surveys that happened to fall in the SDSS footprint, and hence had available $g - r$ colors. These stars covered a variety of metallicities, but in particular a large number of stars with [Fe/H] < -1.0 were included. An approximate transformation, suitable for low-metallicity stars, was obtained by Zhao & Newberg (2006); the transform $B - V = 0.187 + 0.916(g - r)$ was employed. In the near future we plan on deriving a new calibration of this method, directly using $g - r$ colors, based on a large set of high-resolution observations of stars that are being obtained at present. This will eliminate the uncertainty inherent in the application of a transformation of colors.

Comparison of the metallicities obtained from this method with those derived from high-resolution spectroscopy of SDSS-I/SEGUE stars, and for member stars of open and globular clusters with known [Fe/H], indicated that [Fe/H] for stars with $g - r > 0.7$ are consistently underestimated (due to saturation of the Ca II K line); we consider only metallicities determined for stars with $0.1 \leq g - r \leq 0.7$ as a valid estimates from this approach.

The Autocorrelation Function technique was developed as an alternative method for metallicity estimation which should perform well at higher metallicities, where the Ca II

K technique is limited by saturation. As described in Beers et al. (1999, and references therein), the method relies on an auto-correlation of a given stellar spectrum, which generates a correlation peak whose strength is proportional to the frequency and strength of weak metallic lines in a given spectrum. The more such lines exist, the stronger the signal. This function has been calibrated as a function of $B-V$ color; as before, a transformation from $g-r$ to $B-V$ is used in order to obtain a prediction of [Fe/H].

The autocorrelation signal is expected to depend strongly on the signal-to-noise of a given spectrum, growing with decreasing S/N. Essentially, in the low S/N limit, this function is responding to noise peaks rather than to the presence of metallic features. This effect can be corrected for, such that the measured S/N over the region in which the autocorrelation function is calculated enters as a part of the calibration, and is effectively subtracted off. We performed such a procedure for a set of SDSS stellar spectra with parameters obtained from an early version of the SSPP. While the Autocorrelation Function method exhibits a rather small star-to-star abundance scatter applied to the spectra of stars from open and globular clusters of known metallicity (indicating that it is performing well), it suffers a significant metallicity offset (0.5 to 1.0 dex too low), suggesting that the initial calibration to the SSPP was suspect. Although we calculate the value of this function during the execution of the SSPP, we do not employ it in the final derived abundance estimates. In the near future, we expect to obtain a re-calibration of this approach, based on the high-resolution spectroscopic observations that have now been carried out. This re-calibration will also be performed directly to $g-r$ colors.

The [Fe/H] estimates from these two approaches are referred to as M4 for the Ca II K method, and as M5 for the Autocorrelation Function technique.

4.3. Calibration of a Ca II Triplet Estimator of Metallicity

The SDSS spectra extend to sufficiently red wavelengths to include the prominent Ca II triplet feature, which covers a spectral region 8,400-8,700 Å. These lines are known to be sensitive to both luminosity (surface gravity) as well as metallicity, so care must be exercised in their use as a metallicity indicator.

We have used a line index that measures the integrated strength of these lines, corrected for the presence of Paschen H lines, which also occur in this wavelength interval. The line index definition, and the calculation of the summed index, is as described by Cenarro et al. (2001a,b). In order to calibrate this index for use with SDSS spectra, we have taken the library of some 700 spectra (and their listed atmospheric parameters) given by Cenarro et

al. (see http: //www.ucm.es/info/Astrof/ellipt/CATRIPLET.html), rebinned the spectra to the SDSS spectral resolution, and calculated the corrected Ca II triplet index. This index, along with their listed de-reddened value of the $B-V$ color, are used as inputs to an artificial neural network procedure in order to predict the estimated [Fe/H]. This procedure is able to reproduce the metallicity of the Cenarro et al. stars to within ± 0.3 dex over the temperature range 4,000 K to 8000 K, with some residual sensitivity to surface gravity.

After significant testing, it was decided that the SDSS spectra in the regions of the Ca II triplet suffered from too much noise (often due to poor sky subtraction) in this region in order to this approach to be implemented in the present SSPP. However, we are now mounting a new effort to better clean the Ca II triplet region of residual sky noise in order to see if this indicator can be salvaged. The [Fe/H] estimated from this method is referred to as M6.

4.4. Calibration of a Gravity Estimator Based on the Ca I (4,227 Å) and Mg I b/H Features

Among the prominent metallic species in stellar spectra, the two that are most sensitive to surface gravity are the Ca I line at 4,227 Å and the Mg I b/H feature around 5170 Å. Both of these lines exhibit sensitivity to metallicity as well. We have adopted the line index measurements and quoted atmospheric estimates of [Fe/H] for the dwarfs and giants in the calibration sample of Morrison et al. (2003), which were measured at a similar spectral resolution to the SDSS (2.5–3.5 Å). Surface gravity estimates for the stars involved in this calibration were obtained from the compilation of Cayrel de Strobel (2001), while $B-V$ colors were obtained from the SIMBAD database.

These indices, along with their de-reddened $B-V$ colors and [Fe/H] are used as inputs to an artificial neural network procedure in order to predict the estimated surface gravity $\log g$. This procedure indicates that the prediction errors of the surface gravity, based on the Ca I and MgH indices are on the order of 0.35 dex and 0.30 dex, respectively.

As indicated by Morrison et al. (2003), these two methods are valid in the color range corresponding to $0.4 \leq g-r \leq 0.9$. The gravity estimated from Ca I 4227 is referred to G4, while that obtained from the MgH feature is referred to as G5.

4.5. Parameters Obtained from the Wilhelm et al. (1999) Procedures

These methods are based on the routines described by Wilhelm, Beers, & Gray (1999; WBG99), to which we refer the interested reader. Extensions of these methods used in the SSPP are described below.

The procedures implemented in the SSPP are optimized for two separate temperature ranges, one for the warmer stars ($g-r \leq 0.25$), and one for the cooler stars with redder colors than this limit. The stellar parameter determinations make use of comparisons to theoretical *ugr* colors and line parameters from synthetic spectra, both generated from ATLAS9 model atmospheres (Kurucz CD-ROM 13). The synthetic spectra used in these procedures were generated using the spectral synthesis routine SPECTRUM (Gray & Corbally 1994).

For the hotter stars, the observed normalized spectra are fit with a Voigt profile to determine the Balmer-line equivalent widths and the $D_{0.2}$ (the line width at 20% below the local pseudo-continuum level) widths for Hδ, Hγ, and Hβ. The combination of Balmer-line equivalent widths, $D_{0.2}$, and $u-g$ and $g-r$ colors are used to establish initial $T_{\rm eff}$ and log g estimates, computed from functional trends in the theoretical model parameters. For stars cooler than $T_{\rm eff} \sim$ 8,000 K, the surface gravity is mainly determined by the $u-g$ color. For hotter stars the surface gravity is primarily determined by the $D_{0.2}$ parameter. A metallicity estimate is determined through the use of a combination of the equivalent width of the Ca II K line and a comparison to synthetic spectral regions that contain other metallic lines. Once an initial abundance is established, the procedure is iterated to convergence in all three stellar parameters.

For the cooler stars, only the $g-r$ color is used to establish an initial estimate of $T_{\rm eff}$. For these stars, log g is determined from the $u-g$ color for stars as cool as $T_{\rm eff}$ = 5,750 K. For stars cooler than this limit, the strength of MgH is compared to synthetic spectra of similar $T_{\rm eff}$ and [Fe/H] through the use of a band strength indicator. The metal abundance is determined by the combination of the Ca II K line strength and a minimum χ^2 comparison to metallic-line regions. The procedure is then iterated to convergence.

For stars with $S/N > 10$, errors on the order of $\sigma(T_{\rm eff})$=225 K, $\sigma(\log\ g)$=0.25 dex, and σ([Fe/H])=0.3 dex can be achieved from this technique. The color range of $g-r$ over which this approach is used for the SSPP is $-0.2 \leq g-r \leq 0.8$. The effective temperature, surface gravity, and [Fe/H] estimated from this technique are referred to as T7, G6, and M7.

4.6. The Neural Network Approach

The SSPP implements a flexible method of regression that provides a global non-linear mapping between a set of inputs (the stellar spectrum $\mathbf{x}_i$) and a set of outputs (the stellar atmospheric parameters, $\mathbf{s} = \{T_{\rm eff}, \log\ g, [{\rm Fe/H}]\}$). This method has been described in detail by Re Fiorentin et al. (2007), to where the interested reader is referred for more details.

In the application here, it should be noted that we have chosen not to include input photometry, although this certainly could be added if desired. We build an RR regression model (which means we are training the approach based on real, as opposed to synthetic, spectra) to parameterize real spectra. The training and evaluation data sets are taken from a set of 38,731 stars from 140 SEGUE plates, in directions of low reddening, which have had atmospheric parameters estimated by a preliminary version of the SSPP. This step, which one might think of as "internal training," is clearly not optimal, as one would ideally like an independent basis for the training. This was not possible until recently due to the absence of an adequate noise model for SDSS spectra. Such a model has now been developed; we are in the process of testing and evaluation its use in combination with a new grid of synthetic spectra, and anticipate implementing it in future versions of the neural network approach.

Figure 3 compares our model estimates with those from the early version of the SSPP on the evaluation set. Overall we see good consistency, especially for stars with $T_{\rm eff} < 8,000$ K ($\log\ T_{\rm eff} = 3.90$). Above this effective temperature we see that our models underestimate $\log\ T_{\rm eff}$ relative to the SSPP. Our regression models are designed to interpolate, rather than extrapolate. Extrapolation of the model to estimate atmospheric parameters that are not spanned by the training set is relatively unconstrained. Furthermore, the accuracy of the RR model is limited by the accuracy of the target atmospheric parameters used in training, as well as their consistency across the parameter space. In this case, the SSPP estimates are combinations from several estimation models, each of which operates only over a limited parameter range. Thus, the transition we see above 8,000 K may indicate a temperature region where one of the SSPP sub-models is dominating the SSPP estimates, and this is not well-generalized by our model. From this comparison, we find that the accuracies of our predictions (mean absolute errors) for each parameter are $\sigma(T_{\rm eff}) = 170$ K, $\sigma(\log g) = 0.36$ dex, and $\sigma([{\rm Fe/H}]) = 0.19$ dex.

The RR model has the advantage that exactly the same type of data are used in the training and application phases, thus eliminating the issue of discrepancies in the flux calibration or cosmic variance of the two samples. Of course, this requires an independent estimation method ("basis parameterizer") to parameterize the training templates (which itself must use synthetic models at some level). Our regression model then automates and – more importantly – generalizes this basis parameterizer. Indeed, the basis parameterizer

may even comprise multiple algorithms, perhaps operating over different parameters ranges or used in a voting system to estimate atmospheric parameters. This is true in the present case, where the basis parameterizer comes from a preliminary version of the SSPP.

Experience with the behavior of the neural network approach on the SDSS-I/SEGUE data indicated that this method tends to underestimate [Fe/H] below $T_{\rm eff}$ = 5,000 K and above $T_{\rm eff}$ = 7,500 K, so we restrict its application to this range of temperature, which corresponds to $0.1 \leq g - r \leq 0.7$. Estimates of $T_{\rm eff}$, log g, and [Fe/H] obtained from the neural network approach are referred to as T7, G3, and M3, respectively.

4.7. The χ^2 Minimization Technique Using the NGS1 and NGS2 Grids

4.7.1. Grids of Synthetic Spectra

We have made use of Kurucz's NEWODF models (Castelli & Kurucz 2003), which employs solar abundances from Grevesse & Sauval (1998), to generate two sets of grids of synthetic spectra. The model atmospheres that we used assume plane-parallel line blanketed model structures in one dimensional local thermodynamical equilibrium (LTE), and an enhancement of alpha-element abundances by +0.4 dex for stars with [Fe/H] ≤ -0.5. These new models include H_2O opacities, an improved set of TiO lines, and no convective overshoot (Castelli, Gratton, & Kurucz 1997).

In order to produce the synthetic spectra we employed the TURBOSPECTRUM synthesis code (Alvarez & Plez 1998) with solar abundances by Asplund, Grevesse & Sauval (2005), which uses the treatment of line broadening described by Barklem & O'Mara (1998). The sources of atomic lines used by TURBOSPECTRUM come from largely from the VALD database (Kupka et al. 1999). The molecular species CH, CN, OH, TiO, and CaH are provided by B. Plez (see Plez & Cohen 2005, private communication), while the lines of NH, MgH, and the C_2 molecules are adopted from the Kurucz line lists (see http: //kurucz.harvard.edu/LINELISTS/LINESMOL/). The grid of the synthetic spectra produced have resolutions of 0.01 Å or 0.005 Å, and span 3,500 K $\leq T_{\rm eff} \leq$ 10,000 K in steps of 250 K, from $0.0 \leq \log g \leq 5.0$ in steps of 0.25 dex, and from $-4.0 \leq$ [Fe/H] $\leq +0.5$ in steps of 0.25 dex . These synthetic spectra are referred to as the NGS1 grid. After their generation, these synthetic spectra were degraded to the SDSS resolution $R = 2000$, using a Gaussian convolution algorithm, and the sampled into 1 Å pixels for application of the spectral matching technique described below.

A second grid of model atmospheres was constructed from the Kurucz ATLAS9 models (Castelli & Kurucz 2003), which do not employ alpha-element enhancements for models

with [Fe/H] ≤ -0.5. The TURBOSPECTRUM synthesis code was again used to generate the synthetic spectra. The synthetic spectra have a resolution of 0.1 Å and cover 4,000 K $\leq T_{\rm eff} \leq$ 8,000 K in steps of 250 K, $0.0 \leq \log g \leq 5.0$ in steps of 0.25 dex, and from $-3.0 \leq$ [Fe/H] $\leq +0.5$ in steps of 0.25 dex. Ranges in [α/Fe] were introduced into the spectra, over $-0.2 \leq$ [α/Fe] $\leq +0.8$ in steps of 0.2 dex for each value of $T_{\rm eff}$, log g, and [Fe/H]. These synthetic spectra are referred to as the `NGS2` grid. After their generation, these synthetic spectra are also smoothed to the resolution of the SDSS spectra. The primary purpose of creating the `NGS2` grid is to enable (future) methods for the determination of [α/Fe] for stars in the range 4,000 K $\leq T_{\rm eff} \leq$ 8,000 K. However, since this is an independent grid, it is also possible to obtain another set of predicted stellar atmospheric parameters for the stars within this temperature range.

4.7.2. Pre-processing Observed Spectra for the χ^2 Minimization Technique

The observed SDSS spectra are processed as described in §3 above. The blue region of the spectrum contains most of the information required to constrain the stellar parameters, but for cooler stars, the observed signal-to-noise ratio peaks in the red region. As a compromise, and in order to speed up the analysis, we only consider the spectral range 4,500-5,500 Å. The spectrum under consideration is normalized after obtaining a pseudo continuum over the 4,500-5,500 Å range. The continuum fit is carried out in a similar fashion to that described in §3, but lower order (4th and 3rd) polynomials are employed, due to the shorter wavelength coverage. The synthetic spectra that are used to match with the observed spectra are also normalized in the same fashion over the same wavelength range.

4.7.3. The Parameter Search Technique

We now carry out a search for the best-fit model parameters, i.e., those that minimize the difference between the observed flux vector O and synthetic flux vector S as functions of $T_{\rm eff}$, log g, and [Fe/H] using a reduced χ^2 criteria. That is,

$$\chi^2/DOF = \sum_{i=1}^{m+1} (O_i - S_i)^2/\sigma_i^2 \tag{3}$$

where σ_i is the error in flux in the ith pixel.

To reduce the number of model spectra that must be considered in the calculation of the

the reduced χ^2 values, we first obtain an approximate effective temperature based on a simple approximation. This procedure, which is referred to as the Half Power Point (HPP) method (Wisotzki et al. 2000), obtains an estimate of the wavelength at which the total integrated flux over a spectrum is equal to half of the flux obtained over the entire wavelength region (in this case we use 3,900-8,000 Å). Since the flux distribution for a given stellar spectrum varies rather strongly with effective temperature, once we have determined the HPP wavelength, we are able to obtain a reasonably accurate estimate of effective temperature (or a broadband color such as g - r) by comparing with the HPP wavelengths obtained from a grid of synthetic spectra. The relation between effective temperature and HPP wavelength is established by fitting a cubic polynomial:

$$T_{\rm eff} = (25.63 - 114.51HPP + 177.17HPP^2 - 93.55HPP^3) \times 10,000 \text{ K} \quad (4)$$

where, HPP = wavelength/10,000.

We initially select synthetic spectra over a broad range around this predicted effective temperature, within ±1,500 K. For example, if the HPP predicted temperature of a star is 5,000 K, we consider models between 3,500 K and 6,500 K. As long as the observed spectrum doesn't have a grossly incorrect spectrophotometric calibration, the estimated temperature will be well within this range. We then obtain the reduced χ^2 values between the observed and the selected synthetic spectra over a 4,500-5,500 Å wavelength window.

Considering the distribution of reduced χ^2 as a function of effective temperature only, we now have 360 points (30 different gravities and 18 metallicities) in each temperature grid. We then iteratively clip, in each temperature grid, points that have larger values of reduced χ^2 than the median of the reduced χ^2 values in each grid. This iterative procedure is performed five times, with the clipped values being those that are higher than the median of all surviving values in each step. After this, only a few points in each temperature step are left. Figure 4 shows one example of the result of this procedure. We then fit the reduced χ^2 distribution to a fourth order polynomial function as a function of temperature. At this point, we clip off any points that lie farther than 2σ below and 1σ above the fitted curve. In this manner, we are able to easily find the likely global minimum, instead of becoming stuck in an incorrect local minimum. The adopted effective temperature is taken as the minimum of this fit (shown as the red line in Figure 4).

Once the effective temperature estimate is determined, we are able to narrow down the model grids further. To obtain estimates of [Fe/H] and log g, we select models within ±550 K of the estimated $T_{\rm eff}$, and then employ the same iterative procedure as above, applied to the log g and [Fe/H] values. Note that the values of reduced χ^2 respond sensitively to small

changes in $T_{\rm eff}$ and [Fe/H], allowing for their optimal determinations. However, note that variation in the log g values does not strongly impact the reduced χ^2, due to a shortage of gravity-sensitive lines in the spectral window we examine. This leads to potentially large errors in the estimated log g. These procedures are applied to both the `NGS1` and `NGS2` grids.

Figure 5 shows two examples of synthetic spectra with parameters set to those estimated by the procedure described above, over-plotted on the observed spectral data. The $T_{\rm eff}$, log g, and [Fe/H] estimated from `NGS1` are referred to as T6, G2, and M2, while the log g and [Fe/H] estimated from `NGS2` are referred to as G1 and M1. No independent estimate of $T_{\rm eff}$ is obtained from the `NGS2` grid, as it is essentially degenerate with that determined from the *NGS1 grid*.

4.7.4. Comparisons with Spectral Libraries and Analysis of High-Resolution SDSS-I/SEGUE Stars

In order to validate that the `NGS1` and `NGS2` grid approaches perform well in determining stellar parameter estimates, we compare the results from these techniques with literature values from two spectral libraries (ELODIE; Prugniel & Soubiran 2001, Moultaka et al. 2004) and MILES (Sánchez-Blázquez et al. 2006)), and with those obtained from analysis of the SDSS-I/SEGUE stars with available high-resolution spectroscopy.

Validation from the ELODIE and MILES Spectral Libraries

The spectra in the ELODIE library were obtained with the ELODIE spectrograph at the Observatoire de Haute-Provence 1.93 m telescope, and cover the spectral region 4,000-6,800 Å. We employ 1969 spectra of 1390 stars with a resolving power R = 10,000, which are publicly available as part of the ELODIE 3 release (Moultaka et al. 2004). The spectra are first smoothed with a Gaussian kernel to match the SDSS resolution. Most of the spectra have quite high S/N ratios, and are accompanied with estimated stellar parameters from the literature. Each spectrum (and parameter estimate) has a quality flag ranging from 0 to 4, with 4 being best. In our comparison exercise, we only select stars with 4,000 K $\leq T_{\rm eff} \leq$ 10,000 K with a quality flag ≥ 1 for the spectra and all of the parameters.

Our examination indicates that these two approaches work best in the range 5000 K $\leq T_{\rm eff} \leq$8,000 K. Comparison plots between the literature values and the estimated parameters in this temperature range for 562 stars among the ELODIE spectral library are shown in Figure 6. A Gaussian fit to the residuals of each parameter reveals that the `NGS1` estimate of $T_{\rm eff}$ is higher by 86 K (σ = 96 K), the surface gravity is larger by 0.10 dex (σ = 0.24 dex

), and the metallicity is smaller by 0.17 dex (σ = 0.14 dex) on average. For cooler stars, with 4,000 K $\leq T_{\rm eff} \leq$5,000 K, we find that $< \Delta(T_{\rm eff}) >$ and $< \Delta([{\rm Fe/H}]) >$ are 177 K (σ = 145 K) and 0.09 dex (σ = 0.20 dex), respectively, which are relatively small offsets and scatter, while the $< \Delta(\log {\rm g}) >$ is 0.48 dex with σ = 0.36 dex.

Because the spectra from the ELODIE library are of very high quality, one might wonder how the parameter estimates would compare for the lower S/N data included among the SDSS-I/SEGUE stars. In order to test this, we inject Gaussian noise into the ELODIE spectra to force them to S/N = 50/1, 25/1, 12.5/1, and 6.25/1, respectively, degrade them to the SDSS resolution, and apply the same procedures as above for estimation of the stellar atmospheric parameters. Table 3 shows the results of this exercise. Inspection of this Table shows that, for $S/N \geq 12.5$, the shifts and scatter in the determinations of the parameters remain acceptably small. This has also been confirmed by comparisons with likely members of Galactic star clusters (Lee et al. 2007b).

The MILES library includes 985 spectra obtained with the 2.5m INT and the IDS spectrograph at La Palma. The wavelength coverage is 3,530 $\sim$ 7,430 Å, and the resolution is $\sim$ 2.3 Å (Sánchez-Blázquez et al. 2006). Because the resolution of the spectra is similar to that of SDSS spectra, we employ the original MILES spectra in the analysis. After dropping the spectra with missing parameters and outside 5000 K $\leq T_{\rm eff} \leq$8,000 K, 367 spectra remain. Figure 7 shows the comparison plots between the selected literature values and the parameters estimated from `NGS1` procedure. It is clear from this Figure that offsets and scatter for the three atmospheric parameters are very close to those obtained by comparison with the ELODIE spectral library. For the cooler stars, with 4000 K $\leq T_{\rm eff} \leq$5,000 K, we obtain $< \Delta(T_{\rm eff}) > =$ 179 K with σ = 133 K, $< \Delta([{\rm Fe/H}]) > =$ 0.06 dex with σ = 0.17 dex, and $< \Delta(\log {\rm g}) > =$ 0.58 dex with σ = 0.45 dex.

Very similar behaviors were also found for comparison of the `NGS2` grid technique as for the `NGS1` grid technique. Table 3 summarizes the offsets between the literature values and the estimated parameters for both synthetic grid approaches.

We conclude from these comparisons with the two spectral libraries that estimates of $T_{\rm eff}$ and [Fe/H] over 4,000 K $\leq T_{\rm eff} \leq 8,000\ K$ (corresponding to $0.0 \leq g-r \leq 1.2$) should be acceptable. Surface gravity estimates from these techniques are sufficiently accurate over 5,000 K $\leq T_{\rm eff} \leq$8,000 K (corresponding to $0.0 \leq g-r \leq 0.7$) for both synthetic grid approaches. Both approaches require that, in order to obtain useful parameter estimates, the S/N ratio of the spectra should be larger than S/N = 12.5; for the purpose of the SSPP we conservatively adopt $S/N \geq 20$ in the color range $0.0 \leq g-r \leq 0.4$, and $S/N \geq 10$ in the color range $0.4 \leq g-r \leq 1.2$.

Validation from SDSS-I/SEGUE Stars with Available High-Resolution Spectra

As part of a long-term program to validate, and improve estimates of stellar atmospheric parameters determined by the SSPP, we have obtained higher resolution spectra for over 150 SDSS-I and SEGUE stars over the past two years. The targets cover a wide range of temperature and metallicity, but somewhat less so in surface gravity. Existing "holes" in the parameter space will be given high priority for future high-resolution campaigns. The data have been independently reduced and analyzed by two authors. For a detailed description of these analyses, the interested reader is referred to Allende Prieto et al. (2007). For simplicity of our present comparison, we adopt the mean values of stellar atmospheric parameters obtained by the independent analysis efforts.

Figure 8 shows a comparison between the parameters estimated from the `NGS1` grid approach and those determined from high-resolution analysis, over 5,000 K $\leq T_{\rm eff} \leq$ 8,000 K. As summarized in Table 3, the temperature and surface gravity estimates obtained from `NGS1` are under-estimated by 68 K ($\sigma = 119$ K) and 0.06 dex ($\sigma = 0.28$ dex) dex, respectively; these parameters were offset in the positive direction when compared to the spectral libraries. The average metallicity offset (-0.13 dex) and scatter (0.19 dex) are very close to those obtained by comparison with the two libraries. Considering the results from these three different comparisons, a small systematic offset in our derived metallicities from this method may exist. However, we don't adjust any of these offsets in the current SSPP. Adjustments will be considered for future refinements of the SSPP, once a significant number of additional high-resolution data for SDSS-I/SEGUE stars are obtained.

5. Empirical and Theoretical Predictions of $g-r$ Color and $T_{\rm eff}$

5.1. Predictions of $g-r$ Color

For a variety of reasons (e.g., nascent saturation, difficulties with de-blending of sources, high reddening, etc.), the SDSS PHOTO pipeline (Lupton et al. 2001) occasionally reports incorrect, or less-than-optimal estimates of the broadband colors for a given target. Because several of the methods we employ in the SSPP require a good measurement of (at least) the $g-r$ color, it is useful to check if the reported $g-r$ color is commensurate with that predicted from the flux-calibrated spectrum of the source, or with the strength of spectral lines that correlate with effective temperature. This predicted color can be used to raise a cautionary flag for stars with possibly incorrect reported colors, within some tolerance. We have developed three different methods to predict $g-r$ color in the SSPP, as described below.

5.1.1. Prediction of $g-r$ Color from the Half Power Point Method

The first technique, the Half Power Point method (Wisotzki et al. 2000), has been described in §4.7 above, in connection with refining grid searches of parameter space. Here we obtain an empirical calibration of the (de-reddened) $g-r$ by fitting a functional relationship between the half power point wavelength of spectra for stars with well-measured SDSS colors, and located in regions of high Galactic latitude, where reddening is minimal. The best-fit relationship is of the form:

$$g - r = -3.354 + 4.318HPP + 3.247HPP^2 \tag{5}$$

where, HPP = wavelength/10,000. The expected error in prediction is about 0.08 magnitudes, over a broad range of color.

The predicted color obtained in this fashion is (obviously) also a way to identify stellar spectra with poor spectrophotometric flux calibrations. If the observed color reported by SDSS PHOTO is believed to be correct, and there remains a difference with the color obtained from the above relationship, one might be justifiably concerned about the quality of the spectrophotometric correction that has been applied. Unresolved binaries, especially those involving a red and a blue member, can also be identified by looking for discrepancies between the observed and predicted $g-r$ colors.

5.1.2. Prediction of $g-r$ Color from the Hδ and Hα Lines

The strengths of the Balmer lines of hydrogen are also tightly correlated with $g-r$ color over wide ranges of effective temperature. We have made use of the line indices for Hδ and Hα, as determined by the SSPP, to obtain the following relationships:

$$g - r = 0.469 - 0.058HD24 \tag{6}$$

and

$$g - r = 0.818 - 0.092HA24 \tag{7}$$

where $HD24$ and $HA24$ are the Hδ and Hα line indices calculated over a 24 Å band centered on these lines. Note that since the Hα line is stronger, at a given color, than the Hδ line, it can be used to determine predictions of colors for cooler stars. The Hα line is also located

in a region of the spectrum where one expects generally fewer problems with contamination of the index from nearby metallic features.

5.2. Predictions of $T_{\rm eff}$

Effective temperatures predicted by the observed $g-r$ color, or through the strength of the Balmer lines, are sufficiently accurate to be considered as auxiliary estimators to those methods described in §4. We obtain two theoretical and three empirical temperature estimates during execution of the SSPP.

5.2.1. Theoretical $T_{\rm eff}$ Estimates

Two theoretical temperature estimates are based on grids of synthetic spectra generated using the Kurucz models described above, and by consideration of predicted colors from the Girardi et al. (2004) isochrones. For the temperatures based on Kurucz models, we calculate an estimated $g-r$ color, adopting the SDSS filter and instrumental response functions (Strauss & Gunn 2001), then fit a fourth order polynomial:

$$T_{\rm eff} = 7792.22 - 6586.18(g-r) - 4637.23(g-r)^2 - 1994.29(g-r)^3 - 386.24(g-r)^4 \quad (8)$$

In deriving the above relationship, we take into account stellar models with atmospheric parameters in the range $-2.0 \leq$ [Fe/H] ≤ -0.5 and $3.0 \leq \log g \leq 5.0$, where most SDSS-I/SEGUE stars are found. Stars at the extrema of these ranges will have less than ideal estimates of temperature due to the sensitivity of $g-r$ color to either metallicity, surface gravity, or both. The effective temperature estimated from this relation is referred to as T3.

For the temperature estimates based on the Girardi isochrones, we assume that the stars are all older than 10 billion years, are moderately metal poor (i.e., have metallicites in the range $-1.5 \leq$ [Fe/H] ≤ -0.5, and are subgiants or main-sequence stars, which is true for a great majority of the SDSS-I/SEGUE stars. The relationship below, based on a third order polynomial, is referred to as T4:

$$T_{\rm eff} = 7590.26 - 6191.78(g-r) - 4270.92(g-r)^2 - 1225.12(g-r)^3 \quad (9)$$

5.2.2. Empirical $T_{\rm eff}$ Estimates

Two of the three empirical temperature estimates are derived from the Balmer line strengths, similar to the color estimates discussed above, but calibrated to the effective temperature estimates obtained from the methods discussed in §4. The temperatures estimated from the $HA24$ and $HD24$ indices, via the simple linear relationships below, are referred to as T1 and T2, respectively.

$$T_{\rm eff} = 4133 + 371 HA24 \tag{10}$$

$$T_{\rm eff} = 5449 + 206 HD24 \tag{11}$$

We restrict the regions over which the above relationships are applied to $1.0\,\text{Å} \leq HA24 \leq 12.0\,\text{Å}$ and $1.0\,\text{Å} \leq HD24 \leq 15.0\,\text{Å}$, respectively.

The final empirical temperature estimate comes from the relationship between the effective temperature derived from a previous version of the SSPP and the observed $g-r$ color (Ivezic et al. 2007). The temperature estimated from the relationship below is referred to as T5:

$$\log\ T_{\rm eff} = 3.8820 - 0.3160(g-r) + 0.0488(g-r)^2 + 0.0283(g-r)^3 \tag{12}$$

The above temperature estimates are taken into account by the SSPP provided that the color flag (see below) is not raised, and the expected temperature is beyond the region where the primary estimates derived from the techniques described in §4 apply. That is, they are used when the expected temperature is outside the range 4,500 K $\leq T_{\rm eff} \leq$ 7,500 K.

6. Flags Raised During Execution of the SSPP

It is important that the SSPP be able to identify situations where the quoted atmospheric parameters may be in doubt, or simply to make the user away where possible anomalies might be found in the spectra of a given star. We have designed a number of flags which serve this purpose.

There are two primary categories of flags – critical flags and cautionary flags. Critical flags are discussed below. When a critical flag is raised, the SSPP is set to either ignore the determinations of atmospheric parameters for a given source, or it is forced (in the case of the color flag described below) to take steps that differ from normal processing in an attempt

to rescue this information. Obviously, even when information is salvaged, the presence of a critical flag means the user must be aware that special steps have been taken, and the reported estimated parameters must be viewed with this knowledge in mind. The second category of flags are the cautionary flags, which are provided for user consideration, but are not necessarily cause for undue concern. Indeed, sometimes these flags are raised when all is in fact OK, but the flag has been raised due to a peculiarity in the spectrum that is relatively harmless, and which will not unduly influence the determinations of atmospheric parameters. The user should nevertheless be aware of the existence of these flags.

The flags are combined into a single set of four letters, the meanings of which are summarized in Table 4, and described below in more detail. Four placeholders are used in order to accommodate cases where more than one sort of flag is raised.

The nominal condition for the four letter flag combination is 'nnnn', which indicates that the SSPP is satisfied that a given stellar spectrum (and its reported $g-r$ colors) has passed all of the tests that have been performed, and the stellar parameters should be considered as well determined.

The first letter in this combination is set to one of 10 different values: 'n', 'D', 'd', 'H', 'h', 'l', 'E', 'S', 'V', and 'N'. Their explanations follow:

- 'n': The letter 'n' indicates nominal.
- 'D': The letter 'D' indicates that a comparison of the breadth of the Hδ line at 20% below its continuum, $D_{0.2}$, and the line depth below the continuum, R_c, relative to their expected relationship for "normal stars", provided below, does not apply. The expected relationship is given by:

$$R_{\rm c} = -0.009503 + 0.027740 D_{0.2} - 0.000590 D_{0.2}^2 + 0.000006 D_{0.2}^3 \qquad (13)$$

  If $D_{0.2}$ is greater than 35.0 Å and the predicted $R_{\rm c}$ from the above relationship is less than the measured value, then the star is most likely a white dwarf. This is a critical flag.

- 'd': This flag is raised if $D_{0.2}$ is less than 35.0 Å and the predicted $R_{\rm c}$ from above is less than the measured value. In this case, the star is most likely a sdO or sdB star. This is a critical flag.
- 'H': This flag is raised when the estimated $T_{\rm eff}$ from the SSPP is greater than 10,000 K, and is meant to indicate a hot star. This is a critical flag.

- 'h': This flag is raised if the estimated $T_{\rm eff}$ from the SSPP is greater than 8,000 K, and either of the line indices of He I (at 4026.2 Å) or He I (at 4471.7 Å) is greater than 1.0 Å. This indicates that the star is likely to be a hot star. This is a critical flag.

- 'l': This flag is raised if the SSPP judges the star to have a high likelihood of being a late type star (generally late K, M, or later spectral type), beyond the ability of the present pipeline to determine acceptable atmospheric parameter estimates. The condition used for raising the 'l' flag is that the Na line (5892.9 Å) index, as measured over a 24 Å band centered on this feature, is larger than 10 Å, and the $g - r$ color is greater than 0.80. This is a critical flag.

- 'E': This flag is raised if significant emission lines are detected in a spectrum. This is a critical flag.

- 'S': This flag is raised if the spectrum (according to the header information) is a night sky spectrum. This is a critical flag.

- 'V': This flag is raised when an adequate radial velocity could not be found for a given spectrum. This is a critical flag.

- 'N': This flag is raised if the spectrum is considered noisy at the extremes of the wavelength range (e.g., around Ca II K and the Ca II triplet). This is a cautionary flag.

The flags that are used to fill out the remaining three positions of the four letter flag combination are 'C', 'B', 'G', or 'g', as described below:

- 'C': This flag is raised if the SSPP is concerned that the reported $g-r$ color is incorrect. As mentioned above, we calculate three estimates of predicted $g - r$ colors, based on $HA24$, $HD24$, or the Half Power Point method. For each of these three predicted colors, we find the one which is closest to the reported $g - r$ color based on the photometry. If the difference between the reported color and the closest predicted color is larger than 0.2 magnitudes, the color flag is raised. The SSPP is set up to proceed with its calculations of atmospheric parameters using the predicted $g - r$ color. This flag is always found in the second position of the combination flag parameters. This is a critical flag.

- 'B': This flag is raised if the SSPP is concerned that there exists a strong mismatch between the strength of the predicted Hα line index $HA24$, based on the measured Hδ line index, $HD24$. For the great majority of "normal" stars, the predicted value

of the Hα line index is found to be $HA24 = 2.737 + 0.775HD24$. For stars with significant $HA24$ and $HD24$ measurements (which we take to mean that the values of these indices exceed zero by more than 2σ, where σ is the error in the measured line index), if the difference between the predicted $HA24$ line index and the measured $HA24$ index is larger than 2.5 Å, then the 'B' flag is raised. This flag is always found in the third position of the combination flag parameters. This is a cautionary flag.

- 'G or g': This flag is raised if the SSPP suggests that the star may exhibit a strong ('G') or mild ('g') CH G-band (around 4,300 Å), relative to expectation for "normal" stars. This flag is always found in the fourth position of the combination flag parameters. This is a cautionary flag.

7. The SSPP Decision Tree for Final Parameter Estimation

The SSPP uses multiple methods in order to obtain estimates of the atmospheric parameters for each star over a very wide range in parameter space. Each technique has limitations as to its ability to estimate each parameter, arising from, e.g., coverage of the grids of synthetic spectra, methods used for spectral matching, and their sensitivity to the S/N of the spectrum, the range in parameter space over which the particular calibration used for a given method extends, etc.. Hence, it is necessary to obtain a prescription for the inclusion or exclusion of a given technique for the estimation of a given atmospheric parameter. At present, this is accomplished by the assignment of a null (0, meaning the parameter estimate is dropped), or unity (1, meaning the parameter estimate is accepted) value to an indicator variable associated with each parameter estimated by a given technique. In the future, we plan to obtain an improved weighting scheme for the combinations of the parameter estimates, once the grid of high-resolution spectroscopic determinations of atmospheric parameters is more completely filled out.

The S/N of a given spectrum also plays a role in the final decision as to the estimate of a set of atmospheric parameters, and the techniques used (which differ in their sensitivity to S/N). Table 5 lists the ranges of $g-r$ and S/N where each particular method is considered valid. Note that slightly higher requirements on S/N presently exist for the bluer stars (those with $g-r < 0.3$) due to the inherent weakness of the metallic lines. We are presently exploring whether this requirement can be relaxed in the cases of several estimators. All derived parameters that fall outside of the color and S/N ranges listed in this table, for a given technique, are set to $T_{\rm eff} = -9999$, $\log g = -9.999$, and [Fe/H] $= -9.999$ by the SSPP.

Recall that in cases where the color flag 'C' is raised, the predicted $g-r$ color determined

by the procedures described above is used as an input (rather than the reported color) for the techniques that require this information.

7.1. Decisions on Effective Temperature Estimates

There are five primary temperature estimates obtained by the SSPP, and an auxiliary set of five empirically and theoretically determined estimates. Note that a few of the primary techniques extend to temperatures below $T_{\rm eff}$ below 4,500 K and above 7,500 K, although the accuracy obtained by these are lower than in the interval 4,500 K $< T_{\rm eff} <$ 7,500 K. Thus, for stars with temperatures outside of this interval, we also include the auxiliary temperature estimates (in fact, just those that lie within 3σ of the mean of the full auxiliary set) in assembling the final average estimate of $T_{\rm eff}$.

In cases where the color flag 'C' is raised, we ignore all temperatures which rely on the reported $g-r$ color, and only consider those based on spectroscopy alone (e.g., the spectral matching techniques). A robust average of the accepted temperature estimates (those with indicator variables equal to 1) is taken for the final adopted temperature. An internal robust estimate of the scatter around this value is also obtained.

7.2. Decisions on Surface Gravity Estimates

There are eight methods used to estimate surface gravity by the SSPP. Application of the limits on $g-r$ and S/N eliminates a number of these estimates, and a robust average of the accepted log g estimates (those with indicator variables equal to 1) is taken for the final adopted surface gravity. An internal robust estimate of the scatter around this value is also obtained.

7.3. Decisions on [Fe/H] Estimates

Nine different methods are employed to determined [Fe/H] in the present SSPP. As before, indicator variables of 1 or 0 are assigned to the result from each method, according to whether it not it satisfies the range of validity listed in Table 5. Note that two of the methods, the Autocorrelation Function technique (M5) and the Ca II triplet technique (M6) always have their indicator variables set to 0 at present, until better calibrations for these estimators can be obtained.

Three final values of [Fe/H] are determined from the assembled set of accepted estimators. These are referred to as the biweight[1] [Fe/H], the refined [Fe/H], and the adopted [Fe/H], as described below.

The biweight [Fe/H] is simply a robust average of all accepted estimates of metallicity with indicator variables equal to 1.

The refined [Fe/H] value is determined as follows. First, we select a small region of the (`NGS1`) grid where we find spectra that (globally) most closely match the adopted $T_{\rm eff}$, the adopted log g, and the [Fe/H] from individual techniques with indicator variables equal to 1. As an example, if there exist five estimates of [Fe/H] (with indicator variables of 1) with the adopted $T_{\rm eff}$ and adopted log g, then five synthetic spectra with the same temperature and gravity, but five different metallicities, are selected. We then obtain reduced χ^2 values in two restricted regions of wavelength space in the observed spectrum, relative to the selected synthetic spectra. The regions considered are the Ca II K region (3,900-4,000 Å) and the region surrounding the MgH feature (5,000-5,500 Å). These two regions are selected because they retain the most sensitivity to metallicity for the extrema of the range of [Fe/H] and temperature encountered, i.e., for the most metal-poor/warm or metal-rich/cool stars. We then seek the best matching synthetic spectrum over these regions alone, based on the minimum of reduced χ^2 for both regions, respectively. This match is carried out independently for each region. Once the best matching synthetic spectrum (hence [Fe/H]) among the five selected synthetic spectra is identified, we select the accepted [Fe/H] estimates from the SSPP that lie within $\pm$ 0.15 dex of the [Fe/H] of the best-matching synthetic spectrum in each region. These are then averaged in order to obtain the best available metallicity estimate for each region. At this point we have two averaged estimates of [Fe/H], which may be the same (i.e., the same synthetic spectrum matches both regions equally well), or different.

If the adopted estimate of $T_{\rm eff} < 5{,}300$ K , the refined [Fe/H] estimate is set to the average value obtained from the MgH region. The refined value is also set to the metallicity average obtained from this region for the case where $5{,}300 \leq T_{\rm eff} \leq 6{,}500$ K, and the biweight [Fe/H] is > -1.2. This value is also used when $T_{\rm eff} > 6{,}500$ K and the biweight [Fe/H] is ≥ -0.8.

The refined [Fe/H] is set to the average obtained for the Ca II K region when 5,300 K $\leq T_{\rm eff} \leq$ 6,500 K, and the biweight [Fe/H] is ≤ -1.2, The refined value is also set to the metallicity average obtained from this region for the case where $T_{\rm eff} > 6{,}500$ K and the

[1]The biweight family of estimators smoothly diminish the effects of outliers on the resulting central location ("mean") and scale ("standard deviation"). See Beers, Flynn, & Gebhardt (1990) and references therein.

biweight [Fe/H] is < -0.8.

The adopted [Fe/H] is then set as follows. If the difference between the biweight [Fe/H] and the refined [Fe/H] is less than 0.15 dex, the adopted [Fe/H] is set equal to the biweight [Fe/H]. If the difference exceeds 0.15 dex, the adopted [Fe/H] is set to the average value of the biweight [Fe/H] and the refined [Fe/H] estimators.

8. Validation of Final SSPP Parameter Estimates

We do not yet have at our disposal a completely satisfactory set of external spectral libraries with suitable wavelength coverage and available atmospheric parameter estimates that extends over the full range of parameter space explored by techniques employed by the SSPP. Hence, we are limited to comparison with the sets of parameters obtained from analysis of the high-resolution spectra for SDSS-I/SEGUE stars obtained to date, and with information available from the literature for stars in Galactic open and globular clusters that have been observed by the SDSS. We discuss these comparisons below.

8.1. Validation from High-Resolution Spectroscopy

Table 1 summarizes the high-resolution data for SDSS-I/SEGUE stars obtained to date. Although the stars in this Table cover most of the range explored by the SSPP techniques, there remain gaps in this coverage that we hope to fill in the near future.

As noted above, these data have been reduced and analyzed independently by two of the authors (T.S. and C.A.), making use of different methodologies. Details are discussed by Allende Prieto et al. (2007). Tables 6, 7, and 8 summarize the systematic offsets and scatter obtained for estimates of $T_{\rm eff}$, log g, and [Fe/H] from each of the techniques used by the SSPP, relative to high-resolution analyses carried out individually, and collectively. The differences in the numbers of stars considered independently arises because T.S. (results shown as 'HA1' in the Tables) analyzed all available spectra, while C.A. (results shown as 'HA2' in the Tables) performed analysis only for those stars observed with the Hobby-Eberly Telescope. The rows labeled 'MEAN' in the Tables are averaged results from HA1 and HA2 (for stars in common), and adding in the stars from HA1 where HA2 results were not obtained.

Figures 9, 10, and 11 provide comparisons of the estimates of atmospheric parameters for individual techniques used by the SSPP with those obtained from the high-resolution analysis, for $T_{\rm eff}$, log g, and [Fe/H], respectively. Note that comparisons are given even for

the methods that are not fully implemented by the SSPP at present (e.g., the Autocorrelation Function and Ca II triplet metallicity estimators).

Comparison of the estimated temperatures from the SSPP indicates an overall very satisfactory result, although Table 6 confirms that most individual techniques appear to slightly underestimate the $T_{\rm eff}$ obtained from high-resolution analysis of the same stars, more so for HA1 than for HA2. However, as can also be noted from this Table, the final adopted value of effective temperature from the SSPP shows essentially no offset (+9 K), and a one-sigma scatter of 117 K, both of which are encouragingly small. It is clear from inspection of Figure 9 that additional high-resolution observations are required of stars with both higher and lower temperatures than the present sample. The distribution of the final adopted temperatures appears very well correlated with that of the mean values from the high-resolution analysis in the range of 4,500 K $\leq T_{\rm eff} \leq$ 7,500 K.

Comparison of the estimated surface gravities from the SSPP in Table 7 and Figure 10 reveals that methods G3, G6, and G7 exhibit the highest offsets relative to the high-resolution analyses. The behavior of G3 (which comes from the neural network approach described in §4.6 above), is understood because that network was originally trained on a preliminary version of the SSPP, and hence it "inherited" whatever uncertainties existed in surface gravity estimates at that time. It is not presently clear what reasons, other than just the difficulty of extracting accurate estimates of log g, might explain the large offsets of techniques G6 and G7. Inspection of Figure 10 makes it clear that we could benefit from the inclusion of additional stars with lower surface gravities. Nevertheless, the adopted values for surface gravity by the SSPP are reasonably well distributed around the one-to-one correlation line. The offset and one-sigma scatter in the final adopted estimate of log g are +0.03 dex and 0.26 dex, respectively, which is surprisingly good for this difficult-to-estimate parameter.

Comparison of the estimated metallicities from the SSPP in Table 8 and Figure 11 make it clear why we exclude the estimates M5 (the Autocorrelation Function method) and M6 (the Ca-II triplet method) for the time being. The M5 estimates exhibit large (low) offsets for stars at higher metallicites, and a large overall scatter at lower metallicities (the latter is an expected behavior). The M6 estimates are systematically offset (high) from the expected correlation, and also have a larger scatter than desired. There is also a tendency for M3, the estimate obtained from the neural network method, to underestimate the metallicities of the more metal-rich stars. As mentioned previously, this is understood because of training this technique on a previous version of the SSPP. We are in the process of re-calibrating all three estimators, and expect to implement them in future versions of the SSPP.

Inspection of Figure 11 indicates that we could benefit from the addition of more stars

with intermediate metallicities, as well as for stars at the lowest metallicities. The mean offset (-0.03 dex) and one-sigma scatter (0.22 dex) of the residuals between the SSPP predictions of [Fe/H] and the high-resolution analysis are quite encouraging, at least over the parameter space explored to date.

In summary, based on the sets of parameter comparisons with high-resolution analysis, in the effective temperature range of 4,500 K $\leq T_{\rm eff} \leq$ 7,500 K the SSPP is capable of producing estimates of the atmospheric parameters for SDSS-I/SEGUE stars to precisions of $\sigma(T_{\rm eff})$, $\sigma(\log g)$, and σ([Fe/H] of 117 K, 0.26 dex, and 0.22 dex, respectively, with very small average offsets. It should be kept in mind that the stars for which these comparisons are carried out are among the very brightest observed with SDSS, and the overall precision of parameter determination will decline for fainter stars. We are in the process of quantifying the accuracies and precisions of atmospheric parameter determinations as a function of S/N, and will report on these results in due course.

8.2. Validation from Galactic Open and Globular Clusters

Galactic open and globular clusters provide nearly ideal test beds for validation of the stellar atmospheric parameters estimated by the SSPP. In most clusters, it is expected that the member stars were born simultaneously out of well-mixed, uniform abundance gas at the same location in the Galaxy. Therefore, the member stars should exhibit very similar elemental abundance patterns. During the course of SDSS-I and tests for SEGUE, we have secured photometric and spectroscopic data for the clusters M 13, M 15, NGC 2420, and M 67, and can make use of these clusters for validation of the atmospheric parameters obtained by the SSPP. A more detailed description of this validation can be found in Lee et al. (2007b), to which we refer the interested reader. Here, we briefly report on just the results of the [Fe/H] comparisons as a function of $g-r$ color.

Figure 12 shows, from top to bottom, the SSPP estimated metallicities for likely member stars of M 15, M 13, NGC 2402, and M 67 as a function of $g-r$ color. The solid red line is the literature value of metallicity, reported by Harris (1996) for M 15 and M 13, and Gratton (2000) for NGC 2420 and M 67, while the dashed green line indicates the mean SSPP [Fe/H] for the likely member stars (solid dots). Inspection of this Figure indicates that the SSPP obtains results for M 15 that are about 0.14 dex higher than the literature value, agrees quite well with the intermediate-metallicity clusters, and underestimates the metallicity of M 67 by about 0.3 dex. In addition, their appears to exist a slight trend of declining [Fe/H] with respect to $g-r$ in these determinations, at least for the more metal-rich clusters. Observations of additional clusters, especially of intermediate and near-solar

metallicities, will clearly be helpful.

9. Assignment of Spectral Classifications for Early and Late-Type Stars

It is often useful to group stars into rough MK spectral classifications. It should be kept in mind, however, that for this, and any other exercise of assigning MK spectral types, that the MK system *does not* apply to stars other than Population I. That is, typing of metal-poor Population II stars is, *by definition* not a strictly valid procedure. Nevertheless, the SSPP attempts to carry out this exercise using two approaches. The first is based on the spectral type listed in the ELODIE database for the best template match obtained for the determination of radial velocity (as described above), and applies to stars with spectral classes O to M.

For the coolest stars, measuring precise values of $T_{\rm eff}$, $\log g$, and [Fe/H] from spectra dominated by broad molecular features becomes extremely difficult (e.g., Woolf & Wallerstein 2006). As a result, the SEGUE SSPP does not estimate atmospheric parameters for stars with $T_{\rm eff} < 4500$ K, but instead estimates the MK spectral type of each star using the 'Hammer' spectral typing software developed and described by Covey et al. (2007) [2]. The Hammer code measures 23 spectral indices, including atomic lines (H, Ca I, Ca II, Fe I, Mg I, Na I) and molecular bandheads (CN, G band, TiO, VO, CaH, FeH) as well as a select set of broad-band color-ratios. The best-fit spectral type of each target is assigned by comparison to the grid of indices measured from more than 1000 spectral-type standards derived from spectral libraries of comparable resolution and coverage (Allen & Strom 1995; Prugniel & Soubiran 2001; Hawley et al. 2002; Bagnulo et al. 2003; Le Borgne et al. 2003; Valdes et al. 2004; Sańchez-Blázquez et al. 2006).

Tests of the accuracy of the Hammer code with degraded ($S/N \sim 5$) STELIB (Le Borgne et al. 2003), MILES (Sánchez-Blázquez et al. 2006) and SDSS (Hawley et al. 2002) dwarf template spectra reveal that the Hammer code assigns spectral types accurate to within $\pm$ 2 subtypes for K and M stars. The Hammer code also returns results for warmer stars, but as the set of indices used is optimized for cool stars, typical uncertainties are $\pm$4 subtypes for A-G stars at $S/N \sim 5$; in this temperature regime, SSPP atmospheric parameters are a more reliable indicator of $T_{\rm eff}$.

Given the science goals of, in particular, the SEGUE program, we emphasize two limi-

[2]The Hammer has been made available for community use: the IDL code can be downloaded from http://www.cfa.harvard.edu/ kcovey/

tations to the accuracy of spectral types derived by the Hammer code:

- The Hammer code uses spectral indices derived from dwarf standards; spectral types assigned to giant stars will likely have larger, and systematic, uncertainties.
- The Hammer code was developed in the context of SDSS-I's high latitude spectroscopic program; the use of broad-band color ratios in the indices set will likely make the spectral types estimated by the Hammer particularly sensitive to reddening. Spectral types derived in areas of high extinction (i.e., low-latitude SEGUE plates) should be considered highly uncertain until verified with reddening insensitive spectral indices.

10. Preliminary Distance Estimates

A number of techniques are presently being explored by members of the SEGUE team in order to derive the best available estimates of distances for stars in the SDSS/SEGUE database. Many rely on the existence of either theoretical or (better) empirical transformations of the substantial amount of photometric data that exists for Galactic clusters obtained with photometric systems other than *ugriz*. These will be reported on in due course (Morrison et al. 2007, in preparation). For now, the SSPP assigns preliminary distance estimates for stars of different luminosity classifications based on the empirical fits of Beers et al. (2000) to the observed color-magnitude diagrams of Galactic clusters of different metallicities and with reasonably well-known distances (in the Johnson $V, B-V$ system). For convenience, we use the same transformations as mentioned above, based on the work of Zhao & Newberg (2006); $V = g - 0.561(g-r) - 0.004$, and $B - V = 0.187 + 0.916(g-r)$.

Beers et al. argue that their distances should be accurate to on the order of 10-20%; a typical value of 15% can be adopted for our distance estimates, although this needs to be confirmed with future work.

The SSPP does *not* make a stellar luminosity classification, but rather, it provides the atmospheric parameters (e.g., $T_{\rm eff}$, log g) from which the user can make an appropriate choice. Distance estimates are obtained for the following rough luminosity classes: Dwarf, Main-Sequence Turnoff, Giant, Asymptotic Giant Branch, and Field Horizontal Branch. Note that distance estimates are obtained for all (feasible) cases where a star may fall into one or more of these classifications, but only one of the listed distances is likely to apply to a given star. The choice is up to the user.

Two other methods for distance estimates are obtained by the SSPP. The first is described by Allende Prieto et al. (2006), to which the interested reader is referred for a

detailed description.

The second is based on the isochrones in the *ugriz* system developed by Girardi et al. (2004). Our initial tests of this method did not converge as well as was hoped. Although we will continue to work on this, and other methods, for distance estimates, we do not fully implement the Girardi et al. isochrone approach in the SSPP for the DR-6 (Adelman-McCarthy et al. 2007b) release.

11. Conclusions

We have described the development and execution of the SEGUE Stellar Parameter Pipeline (SSPP), which makes use of multiple approaches in order to estimate the fundamental stellar atmospheric parameters (effective temperature, $T_{\rm eff}$, surface gravity, log g, and metallicity, parameterized by [Fe/H]) for stars with spectra and photometry obtained during the course of the original Sloan Digital Sky Survey (SDSS-I) and its current extension (SDSS-II/SEGUE).

The results of a comparison with high-resolution spectroscopic analysis of over 150 SDSS-I/SEGUE stars suggests that the SSPP is capable of providing estimates of $T_{\rm eff}$, log g, and [Fe/H] to precisions of 117 K, 0.26 dex, and 0.22 dex, respectively, for stars with 4,500 K $\leq T_{\rm eff} \leq$ 7,500 K, with quite small systematic offsets. Additional high-resolution data for stars outside of this temperature range will enable tests for both cooler and warmer stars.

The results of a comparison with likely member stars of a sample of Galactic open and globular clusters indicates that SSPP may slightly overestimate [Fe/H] (by ~ 0.15 dex) for stars with [Fe/H] < -2.0, and underestimate [Fe/H] (by ~ 0.30 dex) for stars with near-solar metallicities. Slight trends of [Fe/H] with $g-r$ are noticed for the higher metallicity clusters as well, although further data will be needed in order to verify this.

Approximate spectral types are assigned for stars, based on two methods, with differing limitations. A preliminary set of distance determinations for each star is also obtained, although future work will be required in order to identify the optimal method.

We conclude that the SSPP determines sufficiently accurate and precise atmospheric parameter estimates, at least for stars in the effective temperature range 4,500 K to 7,500 K, required to carry out detailed explorations of the chemical compositions and kinematics of the thick-disk and halo populations of the Galaxy.

Funding for the SDSS and SDSS-II has been provided by the Alfred P. Sloan Foundation,

the Participating Institutions, the National Science Foundation, the U.S. Department of Energy, the National Aeronautics and Space Administration, the Japanese Monbukagakusho, the Max Planck Society, and the Higher Education Funding Council for England. The SDSS Web Site is http://www.sdss.org/.

The SDSS is managed by the Astrophysical Research Consortium for the Participating Institutions. The Participating Institutions are the American Museum of Natural History, Astrophysical Institute Potsdam, University of Basel, University of Cambridge, Case Western Reserve University, University of Chicago, Drexel University, Fermilab, the Institute for Advanced Study, the Japan Participation Group, Johns Hopkins University, the Joint Institute for Nuclear Astrophysics, the Kavli Institute for Particle Astrophysics and Cosmology, the Korean Scientist Group, the Chinese Academy of Sciences (LAMOST), Los Alamos National Laboratory, the Max-Planck-Institute for Astronomy (MPIA), the Max-Planck-Institute for Astrophysics (MPA), New Mexico State University, Ohio State University, University of Pittsburgh, University of Portsmouth, Princeton University, the United States Naval Observatory, and the University of Washington.

Y.S.L., T.C.B., and T.S. acknowledge partial funding of this work from grant PHY 02-16783: Physics Frontiers Center / Joint Institute for Nuclear Astrophysics (JINA), awarded by the U.S. National Science Foundation. J.E.N acknowledges support from Australian Research Council Grant DP0663562. C.B.J and P.R.F acknowledge support from the Deutsche Forschungsgemeinschaft (DFG) grant BA2163.

REFERENCES

Abazajian, K., et al. 2005, AJ, 129, 1755

Abazajian, K., et al. 2004, AJ, 128, 502

Abazajian, K., et al. 2003, AJ, 126, 2081

Adelman-McCarthy, J. K., et al. 2007a, ApJS, in press

Adelman-McCarthy, J. K., et al. 2007b, in preparation

Allen, L. E., & Strom, K. M. 1995, AJ, 109, 1379

Allende Prieto, C., Beers, T. C., Wilhelm, R., et al. 2006, ApJ, 636, 804

Allende Prieto, C., et al. 2007, in preparation

Alvares, R. & Plez, B. 1998, A&A, 330, 1109

Asplund, M., Grevesse, N., & Sauval, A. J. 2005, EAS Publications Series, 17, 21

Bagnulo, S., et al. 2003, The Messenger, 114, 10

Barklem, P. S. & O'Mara, B. J. 1998, MNRAS, 300, 863

Beers, T. C., Flynn, K., & Gebhardt, C. 1990, AJ, 100, 32

Beers, T. C., Rossi, S., Norris, J. E., Ryan, S. G.,& Shefler, T. 1999, ApJ, 506, 892

Beers, T. C., Preston, G. W., & Shectman, S. A. 1985, AJ, 90, 2089

Beers, T. C., Preston, G. W., & Shectman, S. A. 1992, AJ, 103, 1987

Beers, T. C., et al. 2000, AJ, 119, 2866

Castelli, F. & Kurucz, R. L. 2003, IAU Symposium, 210, A20

Castelli, F., Gratton, R. G., & Kurucz, R. L. 1997, A&A, 318, 841

Cayrel, R. 1988, IAUS, 132, 345C

Cayrel de Strobel, G., Soubiran, C., & Ralite, N. 2001, A&A, 373, 159

Cenarro A.J., Cardiel N., Gorgas J., Peletier R.F., Vazdekis A., & Prada F. 2001a, MNRAS, 326, 959

Cenarro A. J., Gorgas J., Cardiel N., Pedraz S., Peletier R.F., & Vazdekis, A. 2001b, MNRAS, 326, 981

Christlieb, N. 2003, Rev. Mod. Astron., 16, 191

Covey, K. R., et al. 2007, AJ, submitted

Fukugita, M., Ichikawa, T., Gunn, J.E., Doi, M., Shimasaku, K., & Schneider, D.P. 1996, AJ, 111, 1748

Girardi, L., Grebel, E. K., Odenkirchen, M., & Chiosi, C. 2004, A&A, 422, 205

Gratton, R. 2000, ASP Conf. Ser. 198, 225

Gray, R. O. & Corbally, C. J. 1994, AJ, 107, 742

Grevesse, N. & Sauval, A. J. 1998, SSRv, 85, 161G

Gunn, J. E., et al. 1998, AJ, 116, 3040

Gunn, J. E., et al. 2006, AJ, 131, 2332

Harris, W. E. 1996, AJ, 112, 1487

Hawley, S. L., et al. 2002, AJ, 123, 3409

Ivezic, Z., et al. 2007, in preparation

Kupka, F., Piskunov, N., Ryabchikova, T. A., Stemples, H. C., & Weiss, W. W. 1999, A&AS, 138, 119

Kurucz, R. L. 1993, private communication

Kurucz, R. L. 1993, Kurucz CD-ROM 13, ATLAS9 Stellar Atmosphere Programs and 2 km/s grid (Camgridge: SAO)

Le Borgne, J.-F., et al. 2003, A&A, 402, 433

Lee, Y. S., Beers, T. C., Sivirani, T., et al. 2007b, AJ, submitted

Lupton, R., et al. 2001, in ASP Conf. Ser. 238, Astronomical Data Analysis Software and Systems X, ed. F. R. Harnden, Jr., F. A. Primini, and H. E. Payne (San Francisco: Astr. Soc. Pac.), p. 269

Morrison, H. L., Norris, J., Mateo, M., et al. 2003, AJ, 125, 2502

Moultaka, J., Ilovaisky, S. A., Prugniel, P., & Soubiran, C. 2004, PASP, 116, 693

Nelder, J. & Mead, R. 1965, Comput. J., 7, 308

Pier, J.R., et al. 2003, AJ, 125, 1559

Plez, B. & Cohen, J. G. 2005, A&A, 434, 1117

Prugniel, Ph. & Soubiran, C., 2001, A&A, 369,1048

Re Fiorentin, P., Bailer-Jones, C. A. L., Lee, Y. S. et al. 2007, A&A, 467, 1373

Reimers, D. & Wisotzki, L. 1997, Msngr, 88, 14

Sánchez-Blázquez, P., Peletier, R., Jimenez-Vicente, J., et al. 2006, astro-ph/0607009

Schlegel, D. J., Finkbeiner, D. P., & Davis, M. 1998, ApJ, 500, 525

Stoughton, C., et al. 2002, AJ, 123, 485

Strauss, M & Gunn, J. E. 2001, SDSS Data Release 3, Technical Note (Baltimore: STScI), http://www.wdss.org/dr3/instruments/imager/index.html

Valdes, F., Gupta, R., Rose, J. A., Singh, H. P., & Bell, D. J. 2004, ApJS, 152, 251

Wisotzki, L., Christlieb, N., Bade, N., et al. 2000, A&A, 358, 77

Wilhelm, R., Beers, T., & Gray, R. 1999, AJ, 117, 2308 (WBG99)

Woolf, V. M. & Wallerstein, G. W. 2006, PASP, 118, 218

York, D. G., et al. 2000, AJ, 120, 1579

Zhao, C. & Newberg, H. J. 2006, astro-ph/0612034

Table 1. Summary of High-Resolution Spectroscopy for SDSS and SEGUE Stars

Telescope	Instrument	Resolving power	Wavelength coverage (Å)	Number of stars
Keck - I	HIRES	45,000	3,800 $\sim$ 10,000	11
Keck - II	ESI	6,000	3,800 $\sim$ 10,000	25
HET	HRS	15,000	4,400 $\sim$ 8,000	110
Subaru	HDS	45,000	3,000 $\sim$ 8,000	9

Table 2. Complete List of Line Band and Sideband Widths and Format of the Output from the SSPP

Column	Format	Description	Central (Å)	Width (Å)	Red (Å)	Width (Å)	Blue (Å)	Width (Å)
1	A22	spSpec name	...	...	...	...	...	...
2	F8.3	H8 (3)	3889.0	3.0	3912.0	8.0	3866.0	8.0
3	F8.3	H8 (12)	3889.1	12.0	4010.0	20.0	3862.0	20.0
4	F8.3	H8 (24)	3889.1	24.0	4010.0	20.0	3862.0	20.0
5	F8.3	H8 (48)	3889.1	48.0	4010.0	20.0	3862.0	20.0
6	F8.3	Ca II K12 (12)	3933.7	12.0	4010.0	20.0	3913.0	20.0
7	F8.3	Ca II K18 (18)	3933.7	18.0	4010.0	20.0	3913.0	20.0
8	F8.3	Ca II K6 (6)	3933.7	6.0	4010.0	20.0	3913.0	20.0
9	F8.3	Ca II K	3933.6	30.0	4010.0	5.0	3910.0	5.0
10	F8.3	Ca II HK+	3962.0	75.0	4010.0	5.0	3910.0	5.0
11	F8.3	Hϵ	3970.0	50.0	4010.0	5.0	3910.0	5.0
12	F8.3	Ca II K16 (16)	3933.7	16.0	4018.0	20.0	3913.0	10.0
13	F8.3	Sr II	4077.0	8.0	4090.0	6.0	4070.0	4.0
14	F8.3	He I	4026.2	12.0	4154.0	20.0	4010.0	20.0
15	F8.3	Hδ (12)	4101.8	12.0	4154.0	20.0	4010.0	20.0
16	F8.3	Hδ (24)	4101.8	24.0	4154.0	20.0	4010.0	20.0
17	F8.3	Hδ (48)	4101.8	48.0	4154.0	20.0	4010.0	20.0
18	F8.3	Hδ	4102.0	64.0	4154.0	20.0	4010.0	20.0
19	F8.3	Ca I	4226.0	4.0	4232.0	4.0	4211.0	6.0
20	F8.3	Ca I (12)	4226.7	12.0	4257.0	20.0	4154.0	20.0
21	F8.3	Ca I (24)	4226.7	24.0	4257.0	20.0	4154.0	20.0
22	F8.3	Ca I (6)	4226.7	6.0	4257.0	20.0	4154.0	20.0
23	F8.3	CH G-band	4305.0	15.0	4367.0	10.0	4257.0	20.0
24	F8.3	Hγ (12)	4340.5	12.0	4425.0	20.0	4257.0	20.0
25	F8.3	Hγ (24)	4340.5	24.0	4425.0	20.0	4257.0	20.0
26	F8.3	Hγ (48)	4340.5	48.0	4425.0	20.0	4257.0	20.0
27	F8.3	Hγ	4340.5	54.0	4425.0	20.0	4257.0	20.0
28	F8.3	He I	4471.7	12.0	4500.0	20.0	4425.0	20.0
29	F8.3	G-blue	4305.0	26.0	4507.0	14.0	4090.0	12.0
30	F8.3	G-whole	4321.0	28.0	4507.0	14.0	4096.0	12.0

Table 2—Continued

Column	Format	Description	Central (Å)	Width (Å)	Red (Å)	Width (Å)	Blue (Å)	Width (Å)
31	F8.3	Ba II	4554.0	6.0	4560.0	4.0	4538.0	4.0
32	F8.3	$C_{12}C_{13}$	4737.0	36.0	4770.0	20.0	4423.0	10.0
33	F8.3	CC12	4618.0	256.0	4780.0	5.0	4460.0	10.0
34	F8.3	Metal-1	4584.0	442.0	4805.8	5.0	4363.0	5.0
35	F8.3	Hβ (12)	4862.3	12.0	4905.0	20.0	4790.0	20.0
36	F8.3	Hβ (24)	4862.3	24.0	4905.0	20.0	4790.0	20.0
37	F8.3	Hβ (48)	4862.3	48.0	4905.0	20.0	4790.0	20.0
38	F8.3	Hβ	4862.3	60.0	4905.0	20.0	4790.0	20.0
39	F8.3	C_2	5052.0	204.0	5230.0	20.0	4935.0	10.0
40	F8.3	C_2+Mg I	5069.0	238.0	5230.0	20.0	4935.0	10.0
41	F8.3	MgH+Mg I+C_2	5085.0	270.0	5230.0	20.0	4935.0	10.0
42	F8.3	MgH+Mg I	5198.0	44.0	5230.0	20.0	4935.0	10.0
43	F8.3	MgH	5210.0	20.0	5230.0	20.0	4935.0	10.0
44	F8.3	Cr I	5206.0	12.0	5239.0	8.0	5197.5	5.0
45	F8.3	Mg I+Fe II	5175.0	20.0	5240.0	10.0	4915.0	10.0
46	F8.3	Mg I	5183.0	2.0	5240.0	10.0	4915.0	10.0
47	F8.3	Mg I	5170.5	12.0	5285.0	20.0	5110.0	20.0
48	F8.3	Mg I	5176.5	24.0	5285.0	20.0	5110.0	20.0
49	F8.3	Mg I	5183.5	12.0	5285.0	20.0	5110.0	20.0
50	F8.3	Na I	5890.0	20.0	5918.0	6.0	5865.0	10.0
51	F8.3	Na (12)	5892.9	12.0	5970.0	20.0	5852.0	20.0
52	F8.3	Na (24)	5892.9	24.0	5970.0	20.0	5852.0	20.0
53	F8.3	Hα (12)	6562.8	12.0	6725.0	50.0	6425.0	50.0
54	F8.3	Hα (24)	6562.8	24.0	6725.0	50.0	6425.0	50.0
55	F8.3	Hα (48)	6562.8	48.0	6725.0	50.0	6425.0	50.0
56	F8.3	Hα (70)	6562.8	70.0	6725.0	50.0	6425.0	50.0
57	F8.3	CaH	6788.0	505.0	7434.0	10.0	6532.0	5.0
58	F8.3	TiO	7209.0	333.3	7434.0	10.0	6532.0	5.0
59	F8.3	CN	6890.0	26.0	7795.0	10.0	6870.0	10.0
60	F8.3	O I tri	7775.0	30.0	7805.0	10.0	7728.0	10.0

Table 2—Continued

Column	Format	Description	Central (Å)	Width (Å)	Red (Å)	Width (Å)	Blue (Å)	Width (Å)
61	F8.3	K I	7687.0	34.0	8080.0	10.0	7510.0	10.0
62	F8.3	K I	7688.0	95.0	8132.0	5.0	7492.0	5.0
63	F8.3	Na I	8187.5	15.0	8190.0	55.0	8150.0	10.0
64	F8.3	Na I-red	8190.2	33.0	8248.6	5.0	8140.0	5.0
65	F8.3	Ca II (26)	8498.0	26.0	8520.0	10.0	8467.5	25.0
66	F8.3	Paschen (13)	8467.5	13.0	8570.0	14.0	8457.0	10.0
67	F8.3	Ca II	8498.5	29.0	8570.0	14.0	8479.0	10.0
68	F8.3	Ca II (40)	8542.0	40.0	8570.0	14.0	8479.0	10.0
69	F8.3	Ca II	8542.0	16.0	8600.0	60.0	8520.0	20.0
70	F8.3	Paschen (42)	8598.0	42.0	8630.5	23.0	8570.0	14.0
71	F8.3	Ca II	8662.1	16.0	8694.0	12.0	8600.0	60.0
72	F8.3	Ca II (40)	8662.0	40.0	8712.5	25.0	8630.5	23.0
73	F8.3	Paschen (42)	8751.0	42.0	8784.0	16.0	8712.5	25.0
74	F7.3	TiO1	6720.5	5.0	6720.5	5.0	6705.5	5.0
75	F7.3	TiO2	7059.5	5.0	7059.5	5.0	7044.5	5.0
76	F7.3	TiO3	7094.5	5.0	7094.5	5.0	7081.5	5.0
77	F7.3	TiO4	7132.5	5.0	7132.5	5.0	7117.5	5.0
78	F7.3	TiO5	7130.5	9.0	7130.5	9.0	7044.0	4.0
79	F7.3	CaH1	6385.0	10.0	6415.0	10.0	6350.0	10.0
80	F7.3	CaH2	6830.0	32.0	6830.0	32.0	7044.0	4.0
81	F7.3	CaH3	6975.0	30.0	6975.0	30.0	7044.0	4.0
82	F7.3	CaOH	6235.0	10.0	6235.0	10.0	6349.5	9.0
83	F7.3	Hα	6563.0	6.0	6563.0	6.0	6550.0	10.0
84	F6.1	$< S/N >$						
85	A10	RV Flag						

Table 3. Comparison of SSPP Parameters with the ELODIE and MILES Library Parameters and the High-Resolution Values

Grid	Library	S/N	N	$T_{\rm eff}$ $<\Delta>$ (K)	$T_{\rm eff}$ σ (K)	$\log g$ $<\Delta>$ (dex)	$\log g$ σ (dex)	[Fe/H] $<\Delta>$ (dex)	[Fe/H] σ (dex)
NGS1									
	ELODIE	Full	562	86	96	+0.10	0.24	−0.17	0.14
	ELODIE	50.00	543	110	104	−0.01	0.28	−0.20	0.13
	ELODIE	25.00	538	114	118	−0.05	0.32	−0.18	0.16
	ELODIE	12.50	489	146	155	−0.11	0.43	+0.20	0.20
	ELODIE	6.25	370	149	225	−0.16	0.67	+0.47	0.19
	MILES	Full	367	105	109	+0.11	0.34	−0.19	0.18
	HIGHRES	Full	111	−68	119	−0.06	0.28	−0.13	0.19
NGS2									
	ELODIE	Full	557	...	...	+0.12	0.26	−0.23	0.16
	MILES	Full	341	...	...	+0.14	0.30	−0.25	0.15
	HIGHRES	Full	110	...	...	−0.03	0.25	−0.14	0.18

Note. — HIGHRES is the average of the two high-resolution analyses.

Table 4. Brief Descriptions of SSPP Flags

Flag	Comment
n	All appears normal
D	Likely white dwarf
d	Likely sdO or sdB
H	Hot star with $T_{\rm eff} > 10{,}000$ K
h	Helium line detected, possibly very hot star
l	Likely solar abundance, late-type star
E	Emission lines in spectrum
S	Sky spectrum
V	No radial velocity information available
N	Noisy spectrum at extrema
C	The photometric $g - r$ color may be incorrect
B	Unexpected Hα line strength predicted from Hδ
G	Strong G-band feature
g	Mild G-band feature

Table 5. Valid Ranges of Effective temperature, $g-r$ Color, and S/N for Individual Methods in the SSPP

Temperature										
Method	T1	T2	T3	T4	T5	T6	T7	T8	T9	T10
	$HA24$	$HD24$	K-MOD	G-ISO	EMP	`NGS1`	ANN	WBG99	`k24`	`ki13`
$T_{\rm eff}$[1]	4.5 − 8.5	5.5 − 8.5	4 − 10	4 − 10	4 − 8	4 − 8	5 − 7.5	4.5 − 10	5 − 7	5 − 7
$g-r$	0.0 − 0.8	0.0 − 0.6	-0.2 − 1.2	0.0 − 1.2	-0.2 − 1.2	0.0 − 1.2	0.1 − 0.7	−0.2 − 0.8	0.1 − 0.7	0.1 − 0.7
S/N	...	...	...	...	...	> 10.0	> 10.0	> 10.0	> 10.0	> 10.0
S/N $(g-r<0.3)$	...	...	...	...	...	> 20.0[2]	> 15.0	> 15.0	> 15.0	> 15.0
Gravity										
Method	G1	G2	G3	G4	G5	G6	G7	G8		
	`NGS2`	`NGS1`	ANN	CaI	MgH	WBG	`k24`	`ki13`		
$T_{\rm eff}$[1]	5 − 8	5 − 8	5 − 7.5	4.5 − 6	4.5 − 6	4.5 − 10	5 − 7	5 − 7		
$g-r$	0.0 − 0.7	0.0 − 0.7	0.1 − 0.7	0.4 − 0.9	0.4 − 0.9	−0.2 − 0.8	0.1 − 0.7	0.1 − 0.7		
S/N	> 10.0	> 10.0	> 10.0	> 10.0	> 10.0	> 10.0	>10.0	> 10.0		
S/N $(g-r<0.3)$	> 20.0[2]	> 20.0[2]	> 15.0	...	...	> 15.0	> 15.0	> 15.0		
Metallicity										
Method	M1	M2	M3	M4	M5	M6	M7	M8	M9	
	`NGS2`	`NGS1`	ANN	CaII K	ACF	CaII T	WBG	`k24`	`ki13`	
$T_{\rm eff}$[1]	4 − 8	4 − 8	5 − 7.5	5 − 7	...	...	4.5 − 10	5 − 7	5 − 7	
$g-r$	0.0 − 1.2	0.0 − 1.2	0.1 − 0.7	0.1 − 0.7	...	...	−0.2 − 0.8	0.1 − 0.7	0.1 − 0.7	
S/N	> 10.0	> 10.0	> 10.0	> 10.0	...	...	> 10.0	> 10.0	> 10.0	
S/N $(g-r<0.3)$	> 20.0 [2]	> 20.0 [2]	> 15.0	> 15.0	...	...	> 15.0	> 15.0	> 15.0	

[1] $T_{\rm eff}$ is in units of 1,000 K.

[2] This case is $g-r<0.4$

Note. — S/N is the average signal to noise ratio per pixel over 3,850Å to 6,000Å. $HA24$ and $HD24$ are the temperature estimates from the Hα and Hδ line index in 24 Å widths, respectively. The temperature estimated from Kurucz models is referred to as K-MOD; G-ISO is for the Girardi et al. (2004) isochrones. EMP is the temperature determined by equation 12. These temperature estimates are used only if the color flag is not raised and the mean of these five temperature estimates are greater than 7,500 K or less than 4,500 K. ANN is the neural network approach. ACF is the Autocorrelation Function method, and Ca II T is based on the Ca II triplet line index. [Fe/H] estimates from these approaches are not used at by the SSPP at present. WBG99 is the method from Wilhelm, Beers, & Gray (1999).

Table 6. Comparison of $T_{\rm eff}$ Estimates from Individual Methods with Those From Two High-Resolution Analyses

		AD	T1	T2	T3	T4	T5	T6	T7	T8	T9	T10
HA1	N	75	75	75	75	75	75	75	70	75	70	70
	$<\Delta>$	+53	−32	+12	−16	−95	+4	+9	+21	+116	+179	+4
	σ	92	104	162	144	145	146	94	98	173	154	106
HA2	N	137	135	137	137	137	137	135	127	132	127	127
	$<\Delta>$	−30	−150	−33	−103	−167	−78	−78	−75	+	+54	−100
	σ	147	196	291	183	218	196	169	150	215	184	176
MEAN	N	137	135	137	137	137	137	135	127	132	127	127
	$<\Delta>$	+9	−106	−15	−73	−141	−49	−52	−31	+51	+102	−49
	σ	117	158	243	170	190	172	131	104	173	169	118

Note. — 'AD' is the adopted estimate of $T_{\rm eff}$. 'HA1' indicates the analysis performed by T.S.; 'HA2' indicates the analysis performed by C.A.. 'MEAN' is the average of the two analyses. 'N' is the number of stars compared. $<\Delta>$ is the mean from a Gaussian fit to the residuals of $T_{\rm eff}$ between the SSPP and the high-resolution analysis; σ is the standard deviation of the fit.

Table 7. Comparison of log g Estimates from Individual Methods with Those From Two High-Resolution Analyses

		AD	G1	G2	G3	G4	G5	G6	G7	G8
HA1	N	75	69	70	70	32	32	75	70	70
	$<\Delta>$	−0.06	−0.04	−0.10	−0.30	+0.11	−0.15	−0.63	+0.11	+0.06
	σ	0.34	0.30	0.31	0.36	0.41	0.40	0.81	0.39	0.33
HA2	N	135	125	127	127	54	54	132	127	127
	$<\Delta>$	+0.08	+0.03	−0.01	−0.18	+0.16	+0.03	−0.23	+0.31	+0.13
	σ	0.31	0.36	0.37	0.55	0.41	0.25	0.81	0.40	0.45
MEAN	N	135	125	127	127	54	54	132	127	127
	$<\Delta>$	+0.03	+0.03	−0.05	−0.24	+0.18	0.00	−0.33	+0.26	+0.12
	σ	0.26	0.25	0.29	0.44	0.49	0.29	0.80	0.37	0.38

Note. — 'AD' is the adopted estimate of log$g$. 'HA1' indicates the analysis performed by T.S.; 'HA2' indicates the analysis performed by C.A.. 'MEAN' is the average of the two analyses. 'N' is the number of stars compared. $<\Delta>$ is the mean from a Gaussian fit to the residuals of log g between the SSPP and the high-resolution analysis; σ is the standard deviation of the fit.

Table 8. Comparison of [Fe/H] Estimates from Individual Methods with Those from Two High-Resolution Analyses

		AD	BI	RE	M1	M2	M3	M4	M5	M6	M7	M8	M9
HA1	N	75	75	75	74	75	70	69	74	74	75	70	70
	$<\Delta>$	−0.03	−0.02	−0.07	−0.18	−0.16	−0.10	+0.11	−0.44	+0.45	+0.12	0.08	0.09
	σ	0.18	0.16	0.19	0.18	0.19	0.22	0.29	0.17	0.26	0.20	0.17	0.15
HA2	N	135	135	135	133	135	127	125	134	129	132	127	127
	$<\Delta>$	−0.01	0.00	−0.05	−0.08	−0.08	−0.12	+0.10	−0.31	+0.61	+0.16	0.10	0.14
	σ	0.28	0.27	0.30	0.23	0.26	0.30	0.44	0.37	0.51	0.38	0.35	0.30
MEAN	N	135	135	135	133	135	127	125	134	129	132	127	127
	$<\Delta>$	−0.03	−0.03	−0.06	−0.12	−0.11	−0.13	+0.07	−0.35	+0.56	+0.13	0.08	0.10
	σ	0.22	0.21	0.24	0.18	0.20	0.28	0.42	0.31	0.44	0.30	0.27	0.25

Note. — 'AD', 'BI', and 'RE' are the adopted, biweight, and refined estimates of [Fe/H], respectively. 'HA1' indicates the analysis performed by T.S.; 'HA2' indicates the analysis performed by C.A.. 'MEAN' is the average of the two analyses. 'N' is the number of stars compared. $<\Delta>$ is the mean from a Gaussian fit to the residuals of [Fe/H] between the SSPP and the high-resolution analysis; σ is the standard deviation of the fit.

Table 9. Key to Each Column and Format of the Parameter File from the SSPP.

Column	Format	Description
1	A10	Running number
2	A16	SPEC NAME - MJD-Plate-Fiber
3	A3	Initial target type - BHB (Blue Horizontal Branch), CVR (Star Caty Var), WD (White Dwarf), KD (Brown Dwarf), FTO (Serendipity Blue), MD (Serendipity Red), AGB (Serendipity Distant), SER (Serendipity First), HOT (Hot Std), ROS (ROSAT_D), KG (Star Carbon), GD (Star Red Dwarf), LOW (Star Sub Dwarf), RED (Reddening Standard), PHO (Spectrophotometric Standard), QA (Quality Assurance), GAL (Galaxy), QSO (QSO), SKY (SKY), SER (Serendipity Manual)
4	A3	Spectral Type based on HAMMER program. NA-Not Applicable
5	A3	Spectral Type based on ELODIE templates
6	A4	Flag raised for a variety of reasons. Combination of four letters. - First letter : indicates several things n = all appears well D = likely white dwarf selected by $D_{0.2}$ and Rc d = sdO or sdB selected by $D_{0.2}$ and Rc H = too hot for abundance determinations h = Helium line detected l = late-type star with solar abundance E = emission lines noted (usually more than one) S = Sky spectrum, ignore V = Radial velocity missing N = spectrum quite noisy - Second letter : color flag n = $g - r$ color is OK, compared with predicted color C = $g - r$ color could be wrong - Third letter : Balmer flag indicating disagreement between Hα and Hδ = n if normal = B if not

Table 9—Continued

Column	Format	Description
		- Fourth letter : G-band flag = n if normal = G if likely G-band strong relative to expectation = g if mildly G-band strong relative to expectation
7	F8.3	Adopted [Fe/H]; set to −9.999 if none of the techniques used
8	I3	Number of estimators used; set to 0 if none of the techniques used
9	F8.3	Error in the adopted [Fe/H]; set to −9.999 if missing
10	F8.3	Biweight [Fe/H], set to −9.999 if none of the techniques used
11	I3	Number of estimators used; set to 0 if none used
12	F8.3	Error in biweight [Fe/H], set to −9.999 if missing
13	F8.3	Refined [Fe/H], set to −9.999 if none of the techniques used
14	I3	Number of estimators used; set to 0 if none used
15	F8.3	Error in the refined [Fe/H]; set to −9.999 if missing
16	F8.3	M1; [Fe/H], based on `NGS2` grids; set to −9.999 if missing
17	I3	Indicator variable; set to 1 if the technique used or 0 if not
18	F8.3	Error in [Fe/H], based on the technique; set to −9.999 if missing
19	F8.3	M2; [Fe/H], based on `NGS1` grids; set to −9.999 if missing
20	I3	Indicator variable; set to 1 if the technique used or 0 if not
21	F8.3	Error in [Fe/H], based on the technique; set to −9.999 if missing
22	F8.3	M3; [Fe/H], based on ANN; set to −9.999 if missing
23	I3	Indicator variable; set to 1 if the technique used or 0 if not
24	F8.3	Error in [Fe/H], based on ANN; set to −9.999 if missing
25	F8.3	M4; [Fe/H], based on Ca II K line index method; set to −9.999 if missing
26	I3	Indicator variable; set to 1 if the technique used or 0 if not
27	F8.3	Error in [Fe/H], based on Ca II K method; set to −9.999 if missing
28	F8.3	M5; [Fe/H], based on ACF technique; set to −9.999 if missing
29	I3	Indicator variable; set to 1 if the technique valid or 0 if not
30	F8.3	Error in [Fe/H], based on ACF technique; set to −9.999 if missing
31	F8.3	M6; [Fe/H], based on Ca II triplet method; set to −9.999 if missing
32	I3	Indicator variable; set to 1 if the technique used or 0 if not
33	F8.3	Error in [Fe/H], based on Ca II triplet method; set to −9.999 if missing

Table 9—Continued

Column	Format	Description
34	F8.3	M7; [Fe/H], based on the technique by WBG99; set to −9.999 if missing
35	I3	Indicator variable; set to 1 if the technique used or 0 if not
36	F8.3	Error in [Fe/H], based on WBG99's method; set to −9.999 if missing
37	F8.3	M8; [Fe/H], based on `k24` grids; set to −9.999 if missing
38	I3	Indicator variable; set to 1 if the technique used or 0 if not
39	F8.3	Error in [Fe/H], based on `k24` grids; set to −9.999 if missing
40	F8.3	M9; [Fe/H], based on `ki13` grids; set to −9.999 if missing
41	I3	Indicator variable; set to 1 if the technique used or 0 if not
42	F8.3	Error in [Fe/H], based on `ki13` grids; set to −9.999 if missing
43	I6	Adopted $T_{\rm eff}$; set to −9999 if none of the techniques used
44	I3	Number of temperature estimators used; set to 0 if none used
45	I6	Error in the adopted temperature; set to −9999 if none used
46	I6	T1; $T_{\rm eff}$ estimate from $HA24$ line index
47	I3	Indicator variable; set to 1 if the technique used or 0 if not
48	I6	Error in $T_{\rm eff}$, based on the technique; set to −9999 if missing
49	I6	T2; $T_{\rm eff}$ estimate from $HD24$ line index
50	I3	Indicator variable; set to 1 if the technique used or 0 if not
51	I6	Error in $T_{\rm eff}$, based on the technique; set to −9999 if missing
52	I6	T3; $T_{\rm eff}$ estimate from Kurucz models
53	I3	Indicator variable; set to 1 if the technique used or 0 if not
54	I6	Error in $T_{\rm eff}$. based on the technique; set to −9999 if missing
55	I6	T4; $T_{\rm eff}$ estimate from Girardi et al.(2004) isochrones
56	I3	Indicator variable; set to 1 if the technique used or 0 if not
57	I6	Error in $T_{\rm eff}$, based on the technique; set to −9999 if missing
58	I6	T5; $T_{\rm eff}$ estimate from Ivezic et al. (2007)
59	I3	Indicator variable; set to 1 if the technique used or 0 if not
60	I6	Error in $T_{\rm eff}$, based on the technique; set to −9999 if missing
61	I6	T6; $T_{\rm eff}$, based on `NGS2` grids; set to −9999 if missing
62	I3	Indicator variable; set to 1 if the technique used or 0 if not
63	I6	Error in $T_{\rm eff}$, based on `NGS1` grids; set to −9999 if missing
64	I6	T7; $T_{\rm eff}$, based on ANN; set to −9999 if missing

Table 9—Continued

Column	Format	Description
65	I3	Indicator variable; set to 1 if the technique used or 0 if not
66	I6	Error in $T_{\rm eff}$, based on ANN; set to −9999 if missing
67	I6	T8; $T_{\rm eff}$, based on WBG99's method; set to −9999 if missing
68	I3	Indicator variable; set to 1 if the technique used or 0 if not
69	I6	Error in $T_{\rm eff}$, based on WBG99; set to −9999 if missing
70	I6	T9; $T_{\rm eff}$, based on `k24` grids; set to −9999 if missing
71	I3	Indicator variable; set to 1 if the technique is valid, = 0 if not
72	I6	Error in $T_{\rm eff}$, based on `k24` grids; set to −9999 if missing
73	I6	T10; $T_{\rm eff}$, based on `ki13` grids; set to −9999 if missing
74	I3	Indicator variable; set to 1 if the technique used or 0 if not
75	I6	Error in $T_{\rm eff}$, based on `ki13` grids; set to −9999 if missing
76	F8.3	Adopted log g, based on valid techniques used; set to −9.999 if missing
77	I3	Number of log g estimators used; set to 0 if none used
78	F8.3	Error in the adopted log g; set to −9.999 if none of the estimators used
79	F8.3	G1; log g, based on `NGS2` grids; set to −9.999 if missing
80	I3	Indicator variable; set to 1 if the technique used or 0 if not
81	F8.3	Error in log g, based on the technique; set to −9.999 if missing
82	F8.3	G2; log g, based on `NGS1` grids; set to −9.999 if missing
83	I3	Indicator variable; set to 1 if the technique used or 0 if not
84	F8.3	Error in log g, based on the technique; −9.999 if missing
85	F8.3	G3; log g, based on ANN technique; set to −9.999 if missing
86	I3	Indicator variable; set to 1 if the technique used or 0 if not
87	F8.3	Error in log g based on by ANN; set to −9.999 if missing
88	F8.3	G4; log g, based on Ca I feature; set to −9.999 if missing
89	I3	Indicator variable; set to 1 if the technique used or 0 if not
90	F8.3	Error in log g, based on Ca I; set to −9.999 if missing
91	F8.3	G5; log g, based on MgH feature; set to −9.999 if missing
92	I3	Indicator variable; set to 1 if the technique used or 0 if not
93	F8.3	Error in log g, based on MgH line index; set to −9.999 if missing
94	F8.3	G6; log g, based on WBG99's method; set to −9.999 if missing
95	I3	Indicator variable; set to 1 if the technique used or 0 if not

Table 9—Continued

Column	Format	Description
96	F8.3	Error in log g, based on WBG99; set to −9.999 if missing
97	F8.3	G7; log g, based on `k24` grids; −9.999 if missing
98	I3	Indicator variable; set to 1 if the technique used or 0 if not
99	F8.3	Error in log g based on `k24` grids; set to −9.999 if missing
100	F8.3	G8; log g, based on `ki13` grids; set to −9.999 if missing
101	I3	Indicator variable; set to 1 if the technique used or 0 if not
102	F8.3	Error in log g, based on `ki13` grids; set to −9.999 if missing
103	F8.3	[α/Fe] from `NGS2` grids; set to −9.999 if missing
104	I3	Indicator variable, set to 1 if the technique used or 0 if not
105	F8.3	Error in [α/Fe]; set to −9.999 if missing
106	F9.3	Dwarf distance in kpc from Beers et al. (2000); set to −9.999 if missing
107	F9.3	Turnoff distance in kpc from Beers et al. (2000); set to −9.999 if missing
108	F9.3	Giant distance in kpc from Beers et al. (2000); set to −9.999 if missing
109	F9.3	AGB distance in kpc from Beers et al. (2000); set to −9.999 if missing
110	F9.3	FHB distance in kpc from Beers et al. (2000); set to −9.999 if missing
111	F9.3	Distance in kpc from Allende Prieto et al. (2006); set to −9.999 if missing
112	F9.3	Distance in kpc from Girardi et al.(2004) isochrones; set to −9.999 if missing
113	F9.3	Distance (z) from the Galactic plane from average of Allende Prieto et al. distance and distance based on Girardi et al. isochrones; set to −9.999 if missing
114	F8.3	Ca II KP index; set to −9.999 if missing
115	F8.3	G-band GP index; set to −9.999 if missing
116	F8.1	Observed radial velocity based on vacuum scale; set to −999.9 if missing
117	A10	Radial velocity flag (see description of the pipeline for detail)
118	F8.1	Adopted heliocentric radial velocity estimate; set to −999.9 if missing
119	F8.1	Error in the adopted heliocentric radial velocity; set to −999.9 if missing
120	F8.1	Calculated radial velocity, based on IDL code; set to −999.9 if missing
121	F8.1	Error in the calculated RV; set to −999.9 if missing
122	F8.1	Radial velocity from SDSS templates; set to −999.9 if missing
123	F8.1	Error in SDSS template radial velocity determination; set to −999.9 if missing
124	F8.1	Radial velocity estimated from ELODIE template; set to −999.9 if missing

Table 9—Continued

Column	Format	Description
125	F8.1	Error in ELODIE RV; set to −999.9 if missing
126	F8.1	Radial velocity from spec1d pipeline; set to −999.9 if missing
127	F8.1	Error in rv1d; set to −999.9 if missing
128	F8.1	Galactocentric radial velocity based on adopted velocity; set to −999.9 if missing
129	F8.3	g magnitude; set to −9.999 if missing
130	F8.3	V magnitude from $V = g - 0.561(g - r) - 0.004$; set to −9.999 if missing
131	F8.3	$g - r$ color; set to −9.999 if missing
132	F8.3	Adopted $g - r$ color prediction; set to −9.999 if missing
133	F8.3	$g - r$ color prediction from 0.818 - $0.092HA24$; set to −9.999 if missing
134	F8.3	$g - r$ color prediction from 0.469 - $0.058HD24$; set to −9.999 if missing
135	F8.3	$g - r$ color prediction from half power point; set to −9.999 if missing
136	F8.3	$B - V$ color from $B - V = 0.916(g - r) + 0.187$; set to −9.999 if missing
137	F8.3	$B - V$ color predicted color from Balmer lines; set to −9.999 if missing
138	F8.3	$u - g$ color; set to −9.999 if missing
139	F8.3	$r - i$ color; set to −9.999 if missing
140	F8.3	$i - z$ color; set to −9.999 if missing
141	F8.3	Error in u mag in PSF; set to −9.999 if missing
142	F8.3	Error in g mag in PSF; set to −9.999 if missing
143	F8.3	Error in r mag in PSF; set to −9.999 if missing
144	F8.3	Error in i mag in PSF; set to −9.999 if missing
145	F8.3	Error in z mag in PSF; set to −9.999 if missing
146	F8.3	$E(B - V)$ from Schlegel et al. (1998); set to −9.999 if missing
147	F7.1	Average S/N per pixel over the entire wavelength range
148	I3	Quality check on spectrum. 1 for $S/N > 30$, 2 for $20 < S/N \leq 30$, 3 for $15 < S/N \leq 20$, 4 for $10 < S/N \leq 15$, 5 for $5 < S/N \leq 10$,6 for $S/N \leq 5$
149	F12.7	RA in decimal degrees
150	F12.7	DEC in decimal degrees
151	F12.7	Galactic longitude (l) in decimal degrees
152	F12.7	Galactic latitude (b) in decimal degrees

Table 9—Continued

Column	Format	Description
153	F8.3	Reduced χ^2 value in Ca II H & K region (3,900 $\sim$ 4,000 Å)
154	F8.3	Reduced χ^2 value in wavelength region of 4,000 $\sim$ 4,500 Å
155	F8.3	Reduced χ^2 value in wavelength region of 5,000 $\sim$ 5,500 Å

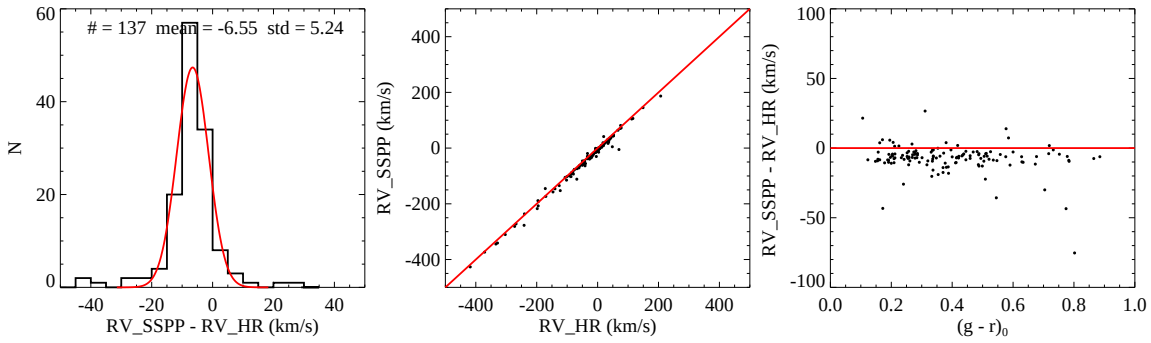

Fig. 1.— A comparison plot of the radial velocity adopted by the SSPP with that measured by the high-resolution analyses. There were three different measurements for stars observed with HET for the high-resolution data. A simple average of the three measurement was taken for this comparison. An offset of -6.6 km s^{-1} is noticed from the Gaussian fit to the residuals. This offset appears constant with $g - r$ in the right panel.

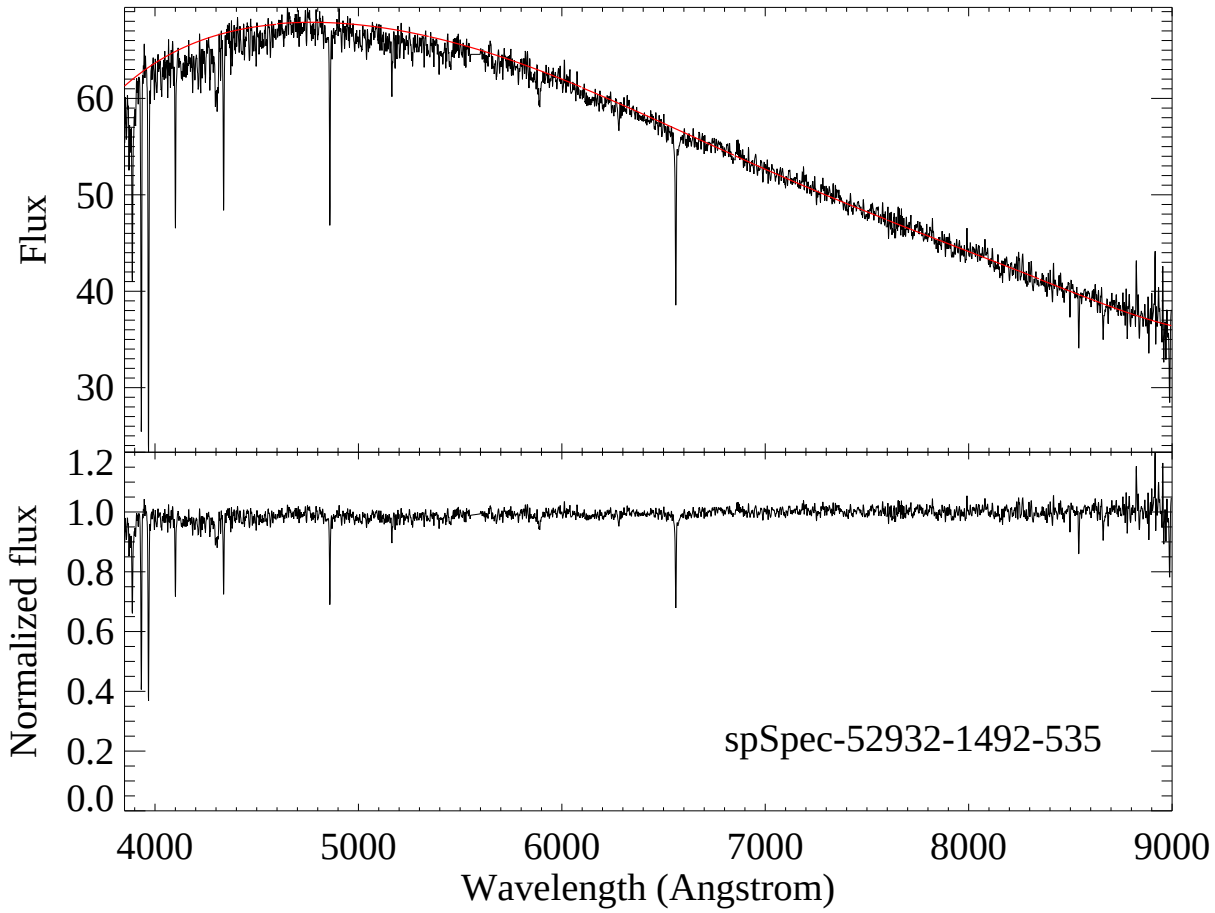

Fig. 2.— An example of a fitted global continuum. The red line in the upper panel is the fitted continuum over the 3,850-9,000 Å wavelength range and the black is the observed spectrum. The bottom panel shows the normalized flux.

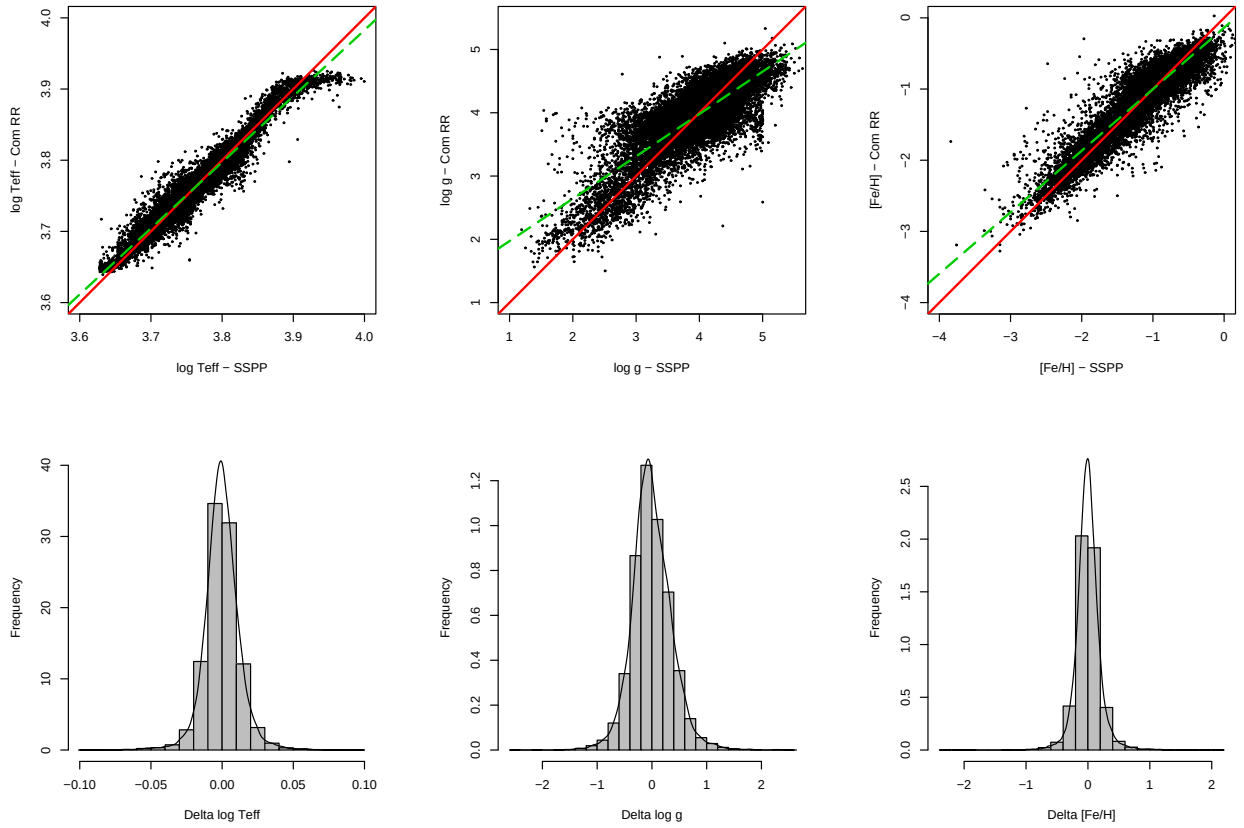

Fig. 3.— Atmospheric parameter estimation with the RR model. We compare our estimated log $T_{\rm eff}$, log g, and [Fe/H] with those from a preliminary version of the SSPP on the 19,000 stars in the evaluation set. The perfect correlation and a linear fit to the data are shown with the solid and dashed lines respectively. The histogram of the discrepancies (our estimates minus SSPP estimates) are shown in the lower panels.

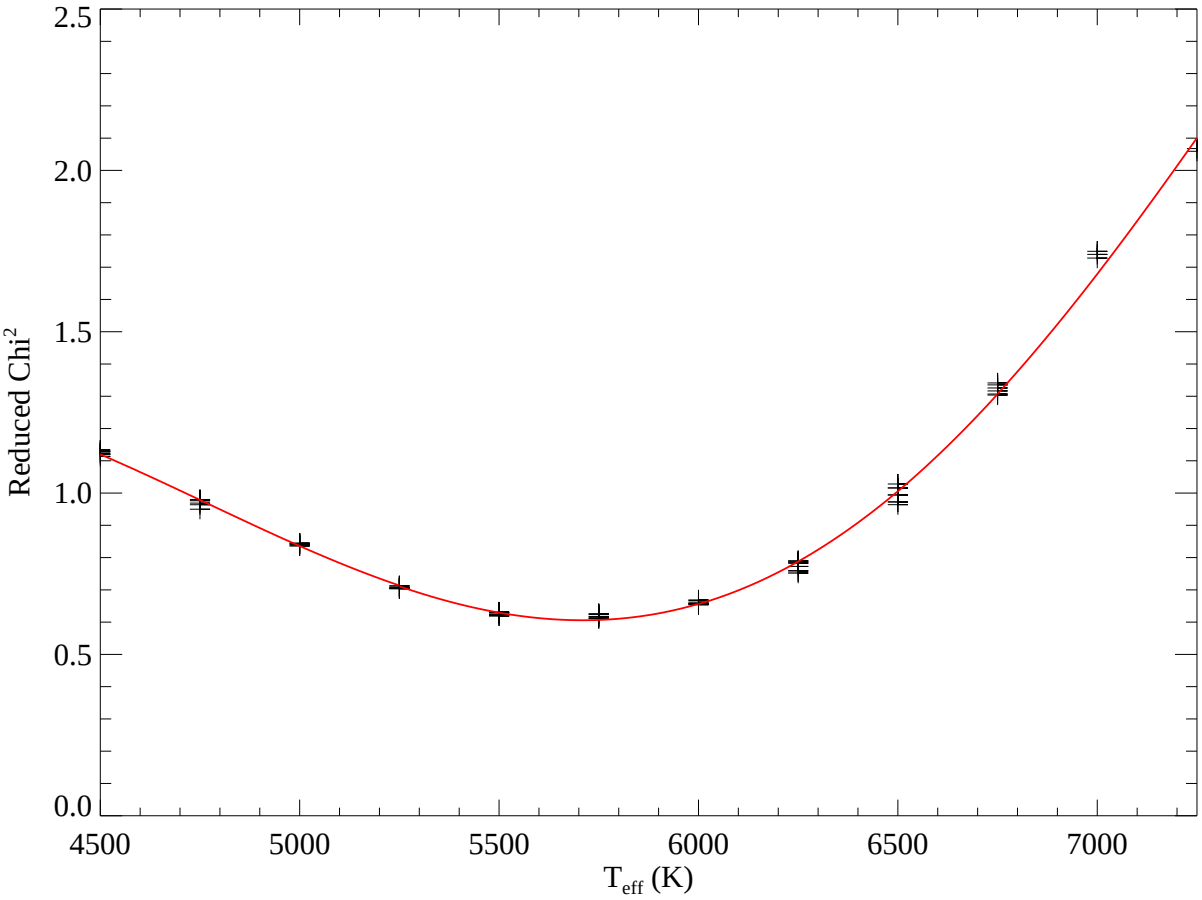

Fig. 4.— An example of finding a minimum reduced χ^2 value as a function of $T_{\rm eff}$. The cross signs are the remaining values after application of an iterative rejection scheme. The red curve is the final fitted function.

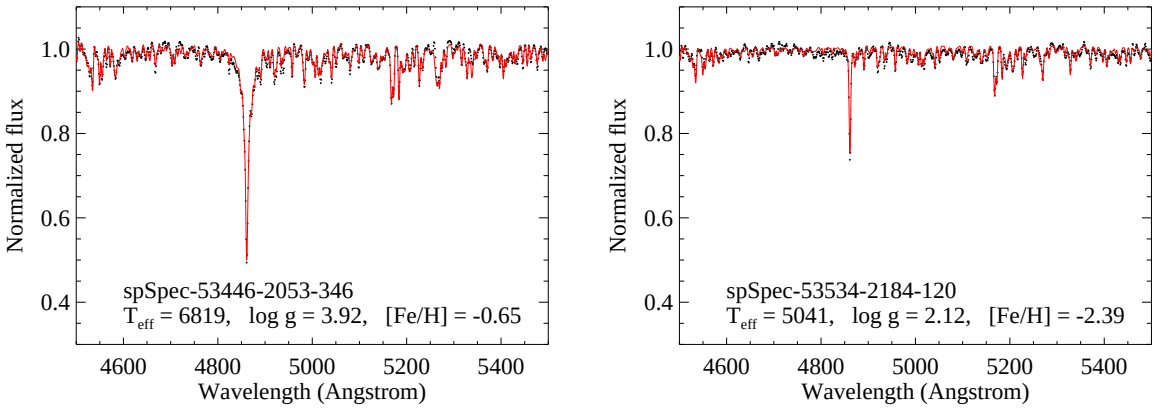

Fig. 5.— Two examples of the results of the application of the SSPP, for a warmer, metal-rich star (left panel), and for a cooler, metal-poor star (right panel). The black dots are the observed data points; the red lines are synthetic spectra generated with the atmospheric parameters adopted by the SSPP.

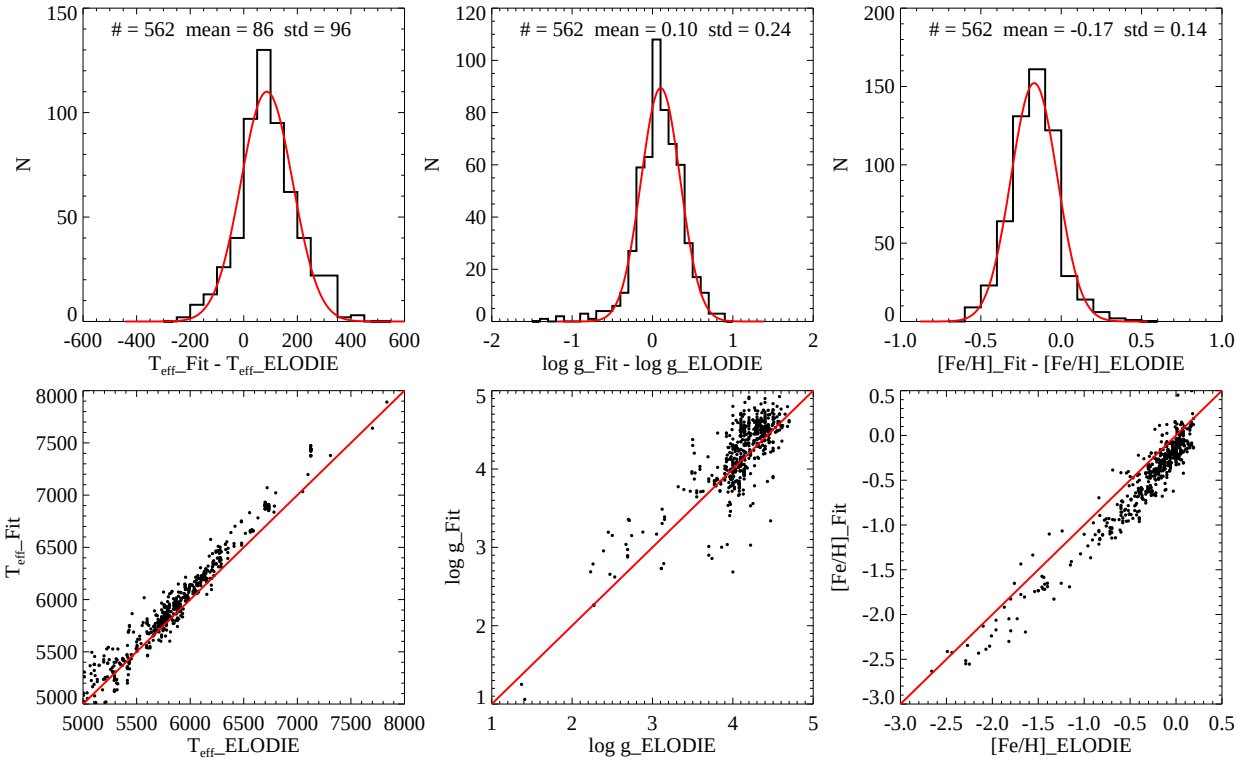

Fig. 6.— Comparison of parameters obtained from the `NGS1` grid (FIT) with those from the ELODIE spectral library (ELODIE). It appears that the temperature and gravity are over-estimated by 86 K and 0.10 dex, respectively, and the metallicity is under-estimated by 0.17 dex, based on Gaussian fits to the residuals.

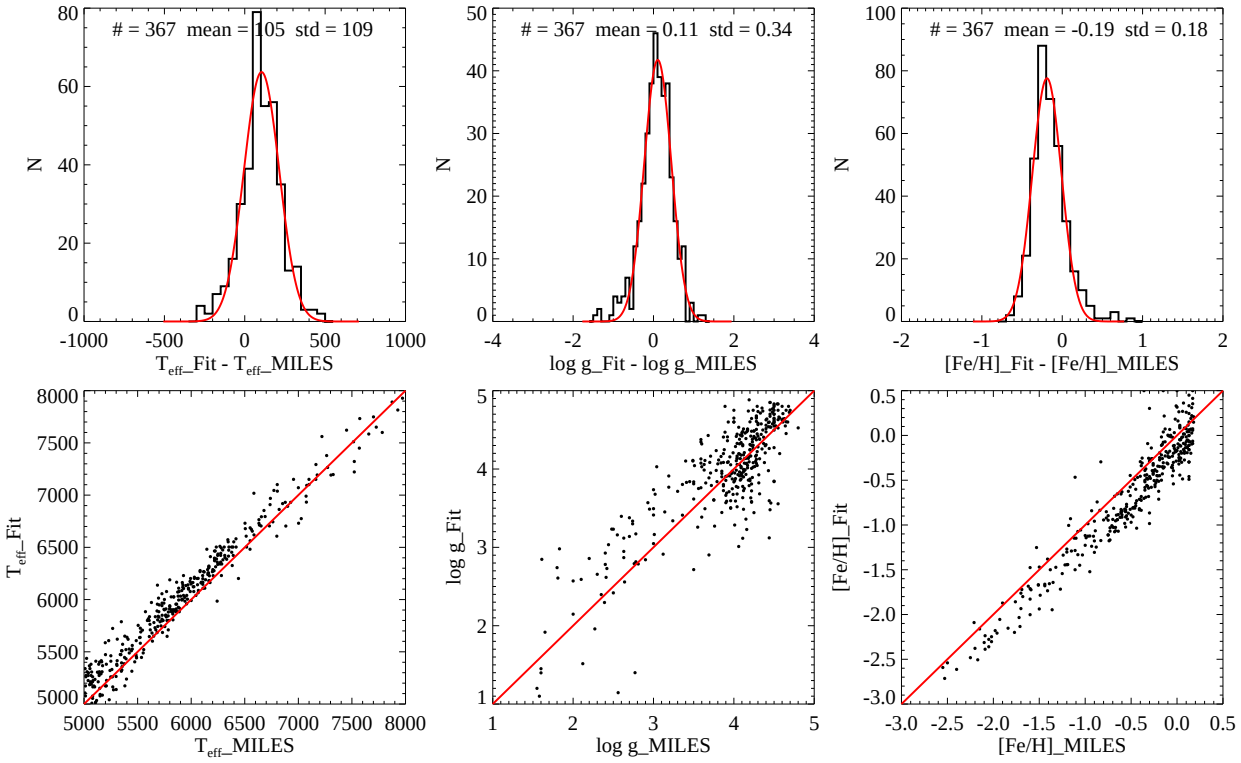

Fig. 7.— Comparison of parameters obtained from the `NGS1` grid (FIT) with those from the MILES spectral library (MILES). It appears that the temperature and gravity are over-estimated by 105 K and 0.11 dex, respectively, and the metallicity is under-estimated by 0.19 dex, based on Gaussian fits to the residuals.

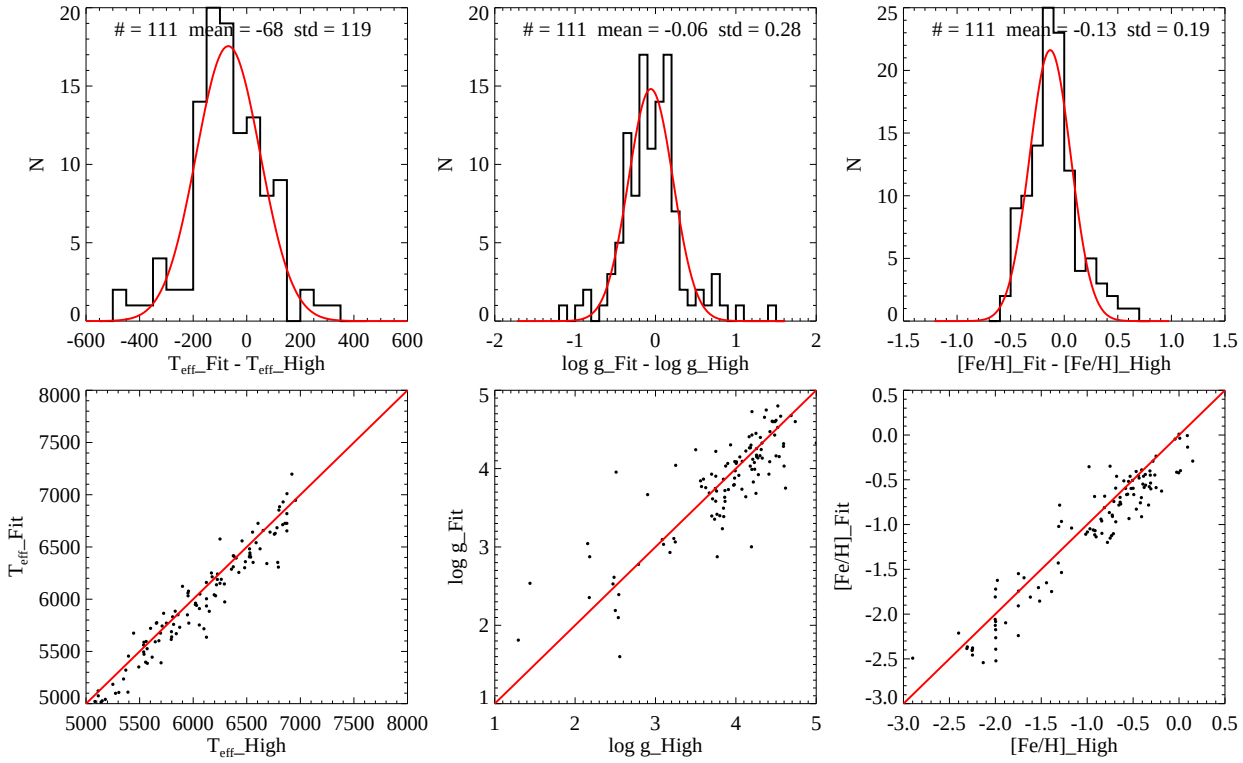

Fig. 8.— Comparison of parameters obtained from the `NGS1` grid (FIT) with those from the analysis of high-resolution spectroscopy of SDSS-I/SEGUE stars (HIGH). The parameters from the high-resolution data are averages of two independent analyses. Contrary to the results from comparisons with the ELODIE and MILES spectral libraries, the effective temperature and the surface gravity are under-estimated, with smaller offsets than those obtained from comparison with the ELODIE and MILES libraries.

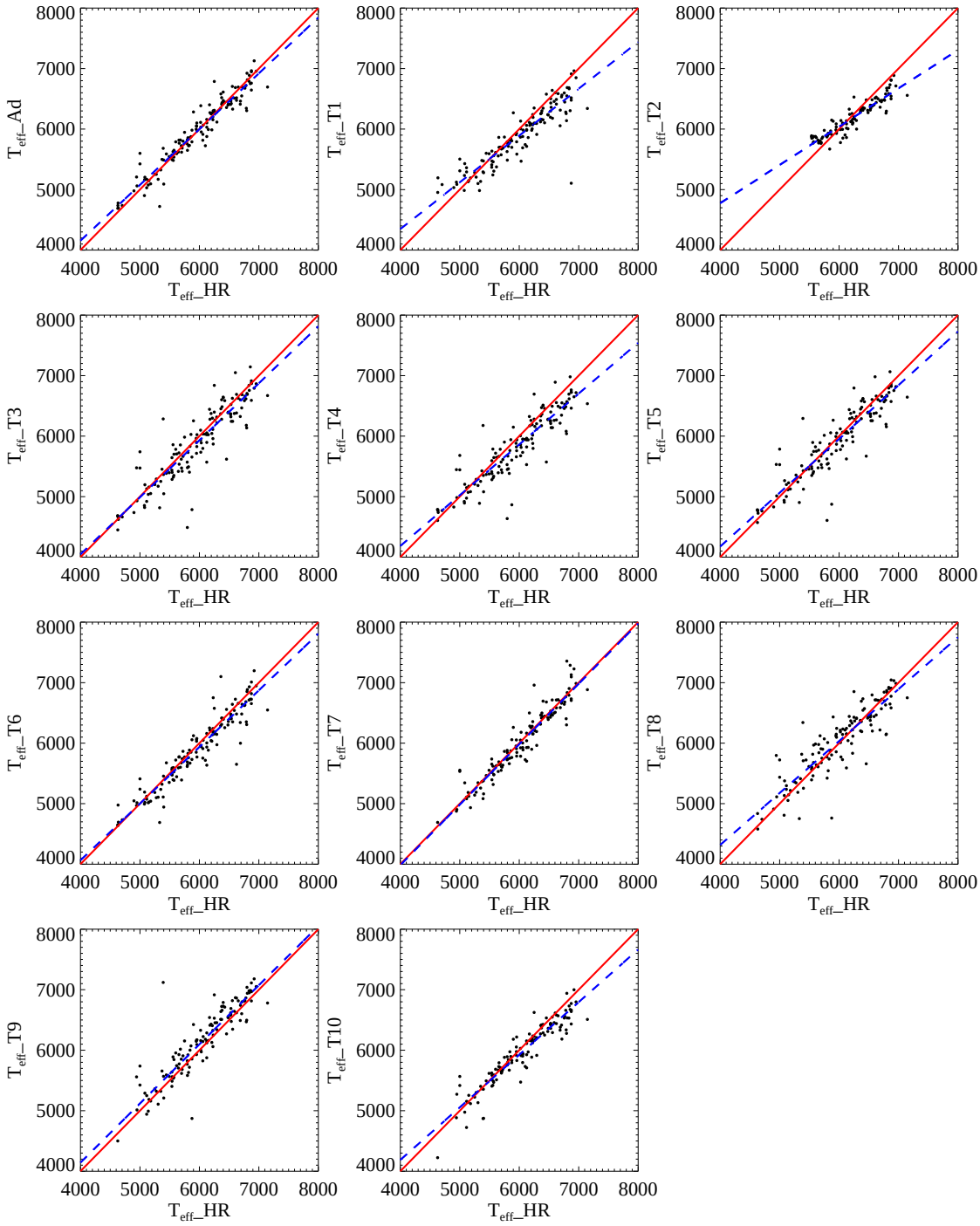

Fig. 9.— Comparison of effective temperatures estimated from individual methods with those from the analysis of high-resolution spectra of SDSS-I/SEGUE stars. 'HR' indicates the high-resolution analysis results. The red solid line is the one-to-one correlation line; the blue dashed line is the least squares fit to the data.

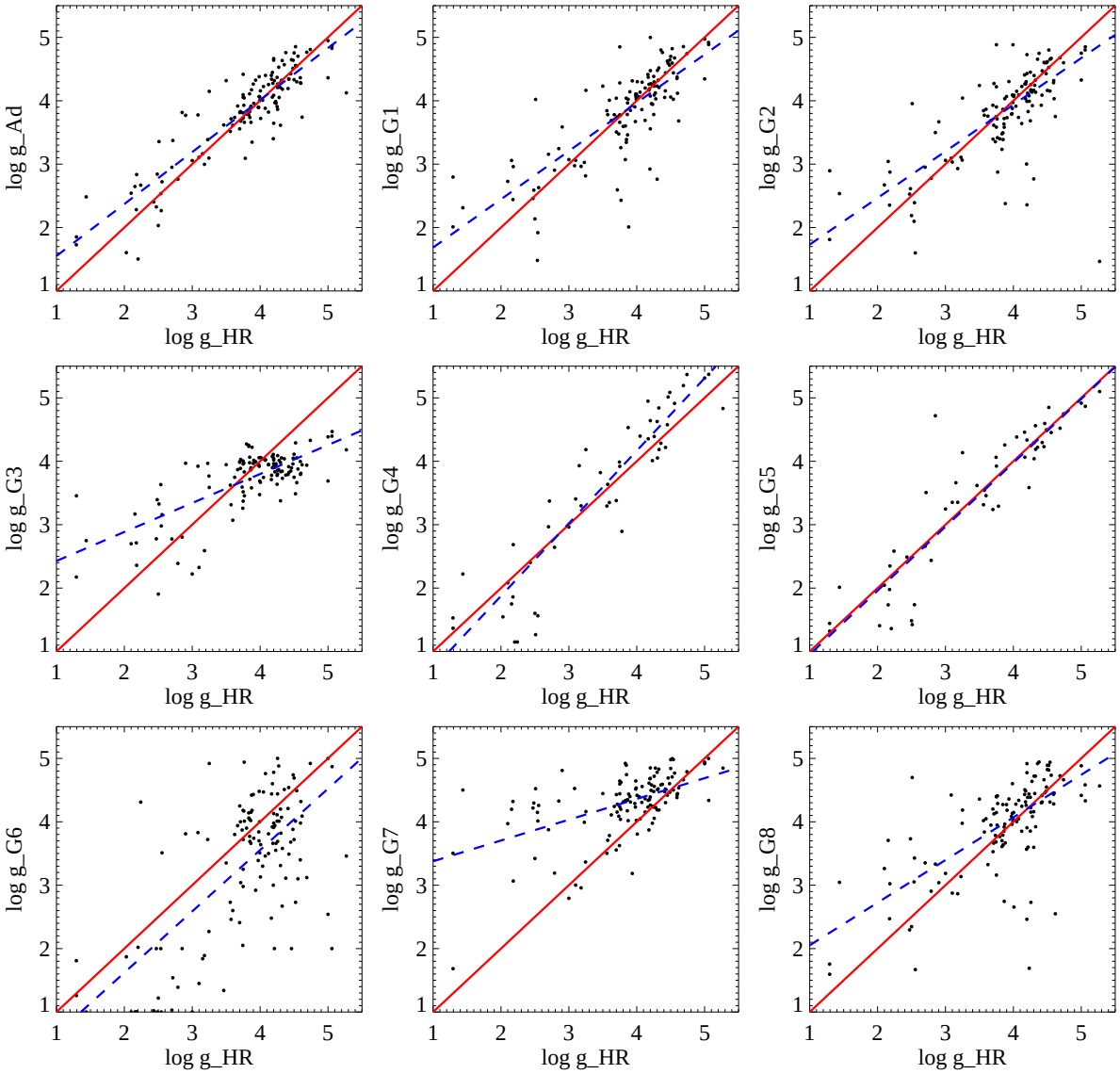

Fig. 10.— Comparison of surface gravities estimated from individual methods with those from the analysis of high-resolution spectra of SDSS-I/SEGUE stars. 'HR' indicates the high-resolution analysis results. The red solid line is the one-to-one correlation line; the blue dashed line is the least squares fit to the data.

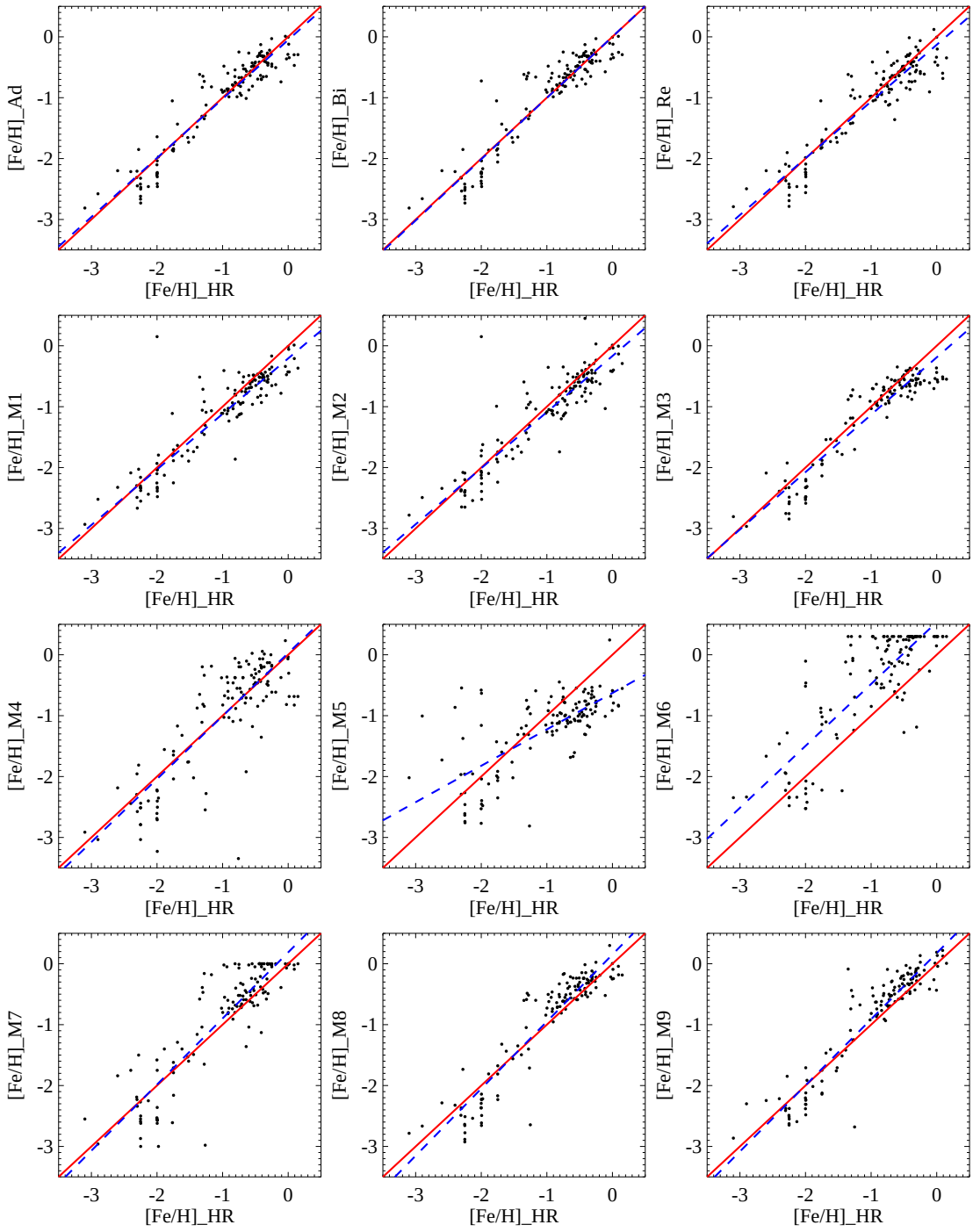

Fig. 11.— Comparison of metallicities estimated from individual methods with those from the analysis of the high-resolution spectra of SDSS-I/SEGUE stars. 'HR' indicates the high-resolution analysis results. The red solid line is the one-to-one correlation line; the blue dashed line is the least squares fit to the data. It is clear why [Fe/H] estimates from M5 and M6 are not taken into account in the final averaging.

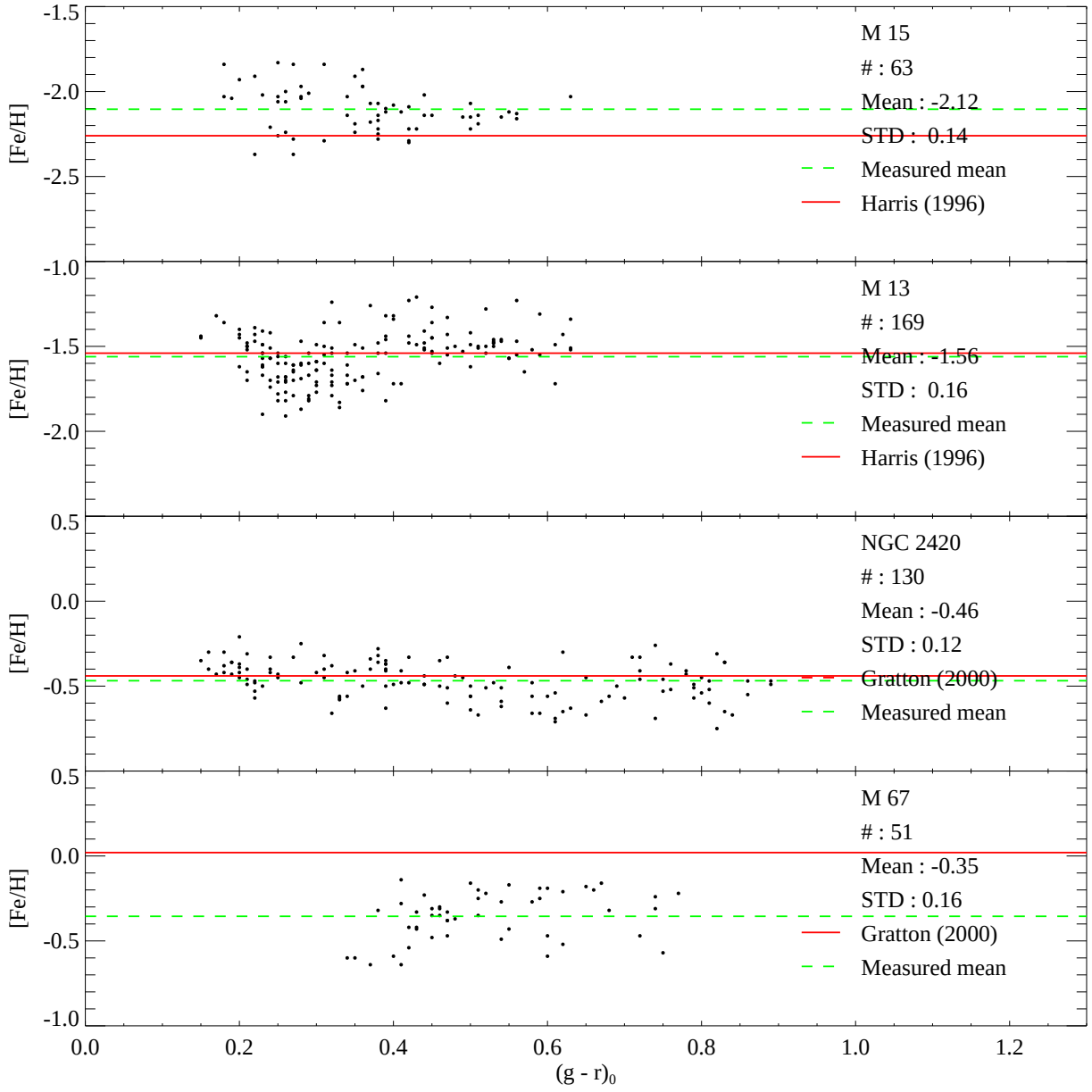

Fig. 12.— SSPP estimated metallicities with respect to $g - r$ for member stars of M 15, M 13, NGC 2420, and M 67. The green dashed line is the Gaussian average of the likely member stars of each cluster. See Lee et al. (2007b) for more detailed selection of member stars and calculation of the Gaussian mean. The red line is the adopted literature value. M 15 and M 13 are taken from Harris (1996); NGC 2420 and M 67 are taken from Gratton (2000).